AIAA Aviation
16-20 June 2014, Atlanta, GA
32nd AIAA Applied Aerodynamics Conference

Parametric Trade Study for Supersonic Bi-Directional Flying Wing

Jiaye Gan*, Alexis Lefebvre†, Daniel Espinal‡, Gecheng Zha§
Dept. of Mechanical and Aerospace Engineering
University of Miami
Coral Gables, FL 33124
gzha@miami.edu

Abstract

This paper conducts a parametric trade study to establish and understand the relationship between the sonic boom/aerodynamic efficiency and the design parameters for supersonic bi-directional flying wing(SBiDir-FW). The mission requirements for this supersonic plane include the cruise Mach number of 1.6, range of 4000 nm, payload of 100 passenger and flight altitude of 50k ft. An advanced geometry model is employed to construct the SBiDir-FW configurations. The geometry model can freely vary airfoil meanline angle distribution to control the expansion and shock waves on the airplane surface in order to mitigate sonic boom and improve aerodynamic efficiency. The trade study has several very important findings: 1) The far field ground sonic boom signature is directly related to the smoothness of the wave distribution on the airplane surface. The meanline angle distribution is a very effective control methodology to mitigate surface shock and expansion wave strength, and mitigate compression wave coalescing by achieving smooth loading distribution chord-wise. Compared with a linear meanline angle distribution, a design using non-monotonic meanline angle distribution with reversed cambering in the mid-chord region is able to reduce the sonic boom ground loudness by over 20PLdB. 2) Decreasing sweep angle within the Mach cone will increase L/D as well as sonic boom. A design with variable sweep from 84° at the very leading edge to 68° at the tip achieves a very high L/D of 10.4 at Mach number 1.6 due to the low wave drag. If no sonic boom constraint is considered, the L/D can be further increased. 3) The round leading edge and trailing edge under high sweep angle are beneficial to improve aerodynamic performance, sonic boom, and to increase volume of the airplane.

The qualitative and quantitative findings in this paper give better understanding of physics and provide the path to achieve the ultimate high performance design. The final

* Ph.D. Candidate
† Ph.D. Candidate
‡ Ph.D. Candidate
§ Professor, AIAA Associate Fellow

design with refined mesh achieves sonic boom ground loudness of 72PldB and aerodynamic dynamic efficiency L/D of 8.3. If increasing the cruise altitude from 50kft to 56kft, the ground sonic boom loudness will be decreased to 68PLdB and 65PLdB respectively. All the design in this study are created manually. It is believed that a systematic automated design optimization will significantly improve the design.

Contents

1 Introduction

Supersonic transports (SSTs) have two major problems: sonic boom and aerodynamic efficiency. Sonic boom is the noise that propagates to ground as an N-wave created by the shock waves of a supersonic airplane. The N-wave represents the sharp pressure rise from the front shock wave, followed by a series of expansion waves, and ends with a shock wave to restore the pressure back to ambient value. The amplitude of N-wave determines the strength of the sonic boom and the annoyance to people. The measured ground N-wave over-pressure amplitude of SR71 propagating from 80,000 ft at Mach 3 is 0.9 psf. Concord has the ground N-wave amplitude of 1.94psf propagating from 52,000 ft altitude at Mach 2. Due to the sonic boom, FAA has banned supersonic flight over land. It is not economic viable for airlines if they can only fly supersonically over sea. Resolving sonic boom issue is hence essential for civil supersonic flight, whereas the aerodynamic efficiency, even though very important, becomes secondary.

One factor affecting aerodynamic efficiency is the extra drag contribution during supersonic flight: the wave drag caused by the entropy increase of strong shock waves. Wave drag does not exist for subsonic airplanes and is not a serious problem for transonic flight due to the low supersonic Mach number. The second factor that affects efficiency is the large flight speed disparity between take-off/landing and cruise. At take-off and landing, the low flight speed requires a high aspect ratio (AR) and low wing sweep angle. High-speed cruise however requires the opposite characteristics. A compromise between low speed take-off/landing and high-speed cruise efficiency is required.

1.1 Overview on Sonic Boom Mitigation

The shock waves contributing to sonic boom are formed by two mechanisms, volume blockage and lift. A solid blockage in a supersonic flow will generate a front shock, followed by an expansion wave due to the diminishing blockage with reduced pressure, which needs to return to ambient pressure through a shock at the end. The pressure variation forms a N-wave that propagates to the ground and produces the sonic boom. However, the strength of the shock waves is determined by the area-weighted distribution of the blockage. The more slender the volume blockage is distributed, the weaker the shock. A very slender body will therefore generate shock waves as weak as isentropic compression wave.

In addition to volume blockage, an airplane must generate lift, which requires high pressure on the lower surface (pressure surface) and low pressure on the upper surface (suction surface). The high pressure will generate compression wave and the low pressure will generate expansion wave. They both propagate downstream within their Mach cone. The compression wave will have slightly higher temperature than the expansion and hence faster wave speed, which is the speed of sound. Away from the airplane in the near field, the pressure wave thus will be measured as the high pressure compression wave in the front and the expansion wave reducing the pressure will follow. Usually, due to the higher curvature on suction surface, the pressure reduction extent by the expansion wave is more than the pressure rise extent of the front compression wave. The pressure downstream of the front compression wave hence will be lower than the ambient pressure. To return the pressure back to ambient pressure, compression waves at the end of the aircraft are needed. Since a compression wave in the downstream always has a higher wave speed and Mach cone angle than the one in the upstream, they have the tendency to merge in the mid-field or far-field to form a shock wave. If both the front and tail compression waves become shock waves,

they appear on the ground as an N-wave. The longer and smoother the lift is distributed, the less intense the compression waves will coalesce. It is possible that the compression waves will not have enough time to coalesce when they reach ground if the pressure compression is smooth and gradual. In that case, we will obtain smooth *Sine* wave shape pressure wave on ground instead of N-wave.

To weaken the shock effect and minimize sonic boom, the dominantly used method at present is to follow the mid-field over pressure signatures suggested by Seebass and George[1, 2, 3] and later further advanced by Darden[4], a flat rooftop shape or a ramp shape. The former is to achieve low ground over-pressure signature and the latter is to achieve weak shock. The flat rooftop shape mid-field over-pressure signature may be achieved by implementing nose bluntness following the area rule theory[5, 6, 3, 2, 7], which is based on linear model for axisymmetric body of revolution and is applied to airplane lifting surface by using equivalent area. A blunt nose design creates a shock distribution in which the greatest shock strengths are near the aircraft and the shocks are weakened gradually due to interaction with expansion waves as the shock waves travel from the aircraft to the ground. Unfortunately, this method also induces substantial wave drag since the entropy increase due to the strong shock waves is irreversible. Darden investigated nose-blunt relaxation as a compromise between the blunt nosed low-boom aircraft and sharp nosed low drag design[8]. McLean found that the pressure signature that reaches the ground from a long slender aircraft with minimal weight change may not fully develop into the far-field N-wave form[9].

The ramp shape mid-field over-pressure signature to mitigate sonic boom is to generate weak leading edge(LE) and trailing edge(TE) shocks, or multiple weak shocks, or ideally isentropic compression waves, to minimize or remove N-wave ground over-pressure signature. For example, designs with sharp nose is for this purpose, which is aerodynamically efficient, but may produce a strong shock at mid-field and far-field distances from the aircraft. In principle, a sharp nose with weak shock or isentropic compression is more likely to achieve both high aerodynamic efficiency and low sonic boom than the nose bluntness method.

In 2008, NASA has outlined the requirements of N+2 (year 2020-2025) and N+3 (year 2030-2035) goal of supersonic civil transport[10]. For N+2, the range $\geq$ 4000nm, Mach number =1.6-2.0, passenger 25-100. For N+3, the range $\geq$ 4000nm, Mach number =1.3-2.0, passenger 100-200. The challenging requirement for both N+2 and N+3 is the sonic boom noise level (based on linear theory) should be between 65 to 70 PLdB. NASA contracted Boeing [11, 12] and Lockheed Martin [13] to conduct design of N+2 supersonic airplane. Both the designs have good aerodynamic performance, but the sonic boom level is at about 80PLdB and are considered as a significant progress on low boom supersonic airplane design.

Automated design optimization plays a very important role in the supersonic airplane design refinement. For example, both the N+2 designs of Boeing[12] and Lockheed Martin[13] are completed with Design of Experiment, which forms a responsive surface based on previous design samples and extracts the optimum. An important progress on design optimization of supersonic airplane is to use adjoint method for gradient calculation originally suggested by Jameson [14, 15]. The research efforts using adjoint method to mitigate sonic boom were first made by Alonson et al [16, 17]. Rallabhandi et al [18] extends the adjoint equation method of NASA FUN3D CFD code to directly calculate the gradient from ground boom signature instead of the near field signature. Rallabhandi further developed a reversed approach to shape an aircraft to equivalent area using discrete adjoint approach. Design optimization can seek an optimum solution efficiently under the design space defined by a design concept. However, it may be difficult to rely on design optimization to find a breaking through new concept.

Zha et al [19, 20, 21, 22] proposed a novel Supersonic Bi-Directional Flying Wing concept (SBiDir-FW) aimed at achieving low sonic boom, minimizing wave drag, maximizing the supersonic and subsonic aerodynamic efficiency and performance. The concept is intended to break through the technical barriers of conventional supersonic tube-wing configurations. The key idea is to render the airplane to achieve ultra-high slenderness at supersonic and high aspect ratio at subsonic low speed to remove the aerodynamic conflict due to speed disparity.

However, since SBiDir-FW is a new concept, no prior knowledge on the correlation between the geometry and sonic boom and aerodynamic performance is available. The purpose of this paper is to conduct parametric trade study to develop such a correlation. A trade study is to vary one design parameter a time and keep all other parameters unchanged to see the effect of that particular parameter. Trade study in general is not able to achieve the global optimum design. However, it is important to conduct the manual trade study to understand the physics and the relationship between the geometry parameters, sonic boom and aerodynamic performance. The trade study will lay a good foundation for further design optimization

2 Supersonic Bi-Directional Flying Wing

The Supersonic Bi-Directional Flying Wing [20, 21, 22] is aimed at breaking through the technical barriers of high sonic boom, poor subsonic performance, and high wave drag of conventional supersonic tube-wing configurations.

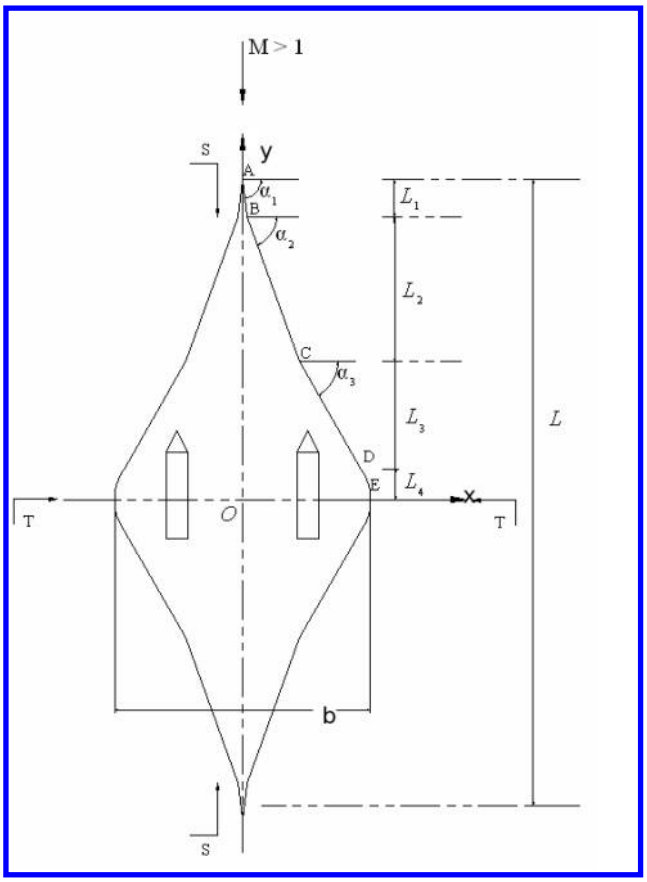

Figure 1: Sketch of a SBiDir-FW Planform flying in supersonic mode (not to scale)

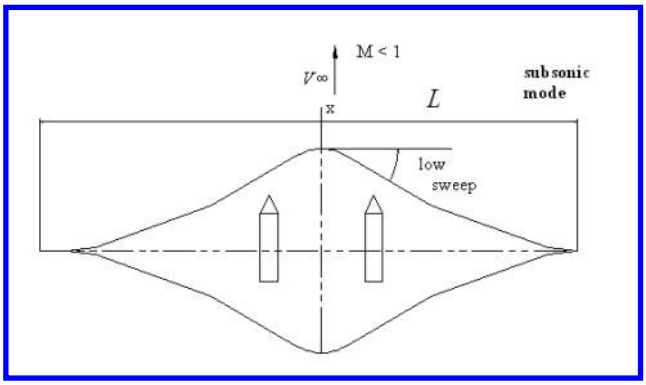

Figure 2: Sketch of a SBiDir-FW Planform flying in subsonic mode (not to scale)

To achieve high aerodynamic efficiency for both supersonic and subsonic, the airplane is a flying wing or blended wing-body configuration with a symmetric planform about both the longitudinal and span axes with two flight directions altered by 90°. At subsonic flight, the planform will rotate 90° from the supersonic mode shown in Fig. 1 to the subsonic mode as shown in Fig. 2. Fig. 4 shows the 3D supersonic flight direction and the thin airfoil highlighted to form the flying wing to achieve low wave drag. Fig. 3 shows the subsonic mode after 90° rotation from the supersonic mode also with the subsonic airfoil highlighted. A reversed rotation will be done when the mode is changed from subsonic to supersonic. Since the span is significantly shorter than the length, the subsonic airfoil will be significantly thicker than the supersonic airfoil as shown in Fig. 3 to provide high lift coefficient needed for subsonic flight.

The engines will not be rotated and will be always aligned with the flight direction. The rotating turbomachinery inside the jet engines also provide the gyroscope effect to enhance the engine stability. The yaw moment to rotate the airframe will be generated by ailerons or flaps on the two sides of the flying wing. No powered driving system like that for swing wing is needed to rotate the airframe and hence the weight penalty and system complication can be avoided. The desirable transition mode Mach number is high subsonic such as about 0.8 to avoid the unsteady force introduced by shock waves at supersonic.

The subsonic aspect ratio will be substantially increased by $(\frac{L}{b})^2$ based on the following relation:

$$AR_{M<1} = ((\frac{L}{b})^2) * AR_{M>1} \tag{1}$$

where L is the airplane length and b its span.

Moreover, the sweep angle at subsonic will be largely reduced as the following:

$$\delta_{M<1} = 90^o - \delta_{M>1} \tag{2}$$

Fig. 3 shows the subsonic flight mode with high aspect ratio and Fig. 4 shows the supersonic flight with a very low aspect ratio after rotation 90^o. To make the flying wing symmetric about both axes, the airfoil stacked is also symmetric as highlighted in Fig. 3 and 4. The symmetric planform will let the trailing edge become leading during the rotation and generate lift to stabilize the mode transition similar to a flying Frisbee. Even though a thin airfoil is used to stack the flying wing in the supersonic direction, sufficient volume can be easily achieved due to the long length of the flying wing body, which is also the chord of the flying wing airfoil.

The SBiDir-FW has the following inherent aerodynamic advantages over the conventional wing-tube configurations.

2.1 Significantly higher slenderness and longer length at Supersonic

Here we define the slenderness coefficient of an object C_s as the following, the greater the value, the higher the slenderness:

$$C_s = V/A_{max}b \tag{3}$$

where V is the total volume, A_{max} is the maximum cross section area normal to the flight direction, and b is the wing span.

Figure 3: A SBiDir-FW civil transport in subsonic mode flying toward right, subsonic thick airfoil highlighted in the middle.

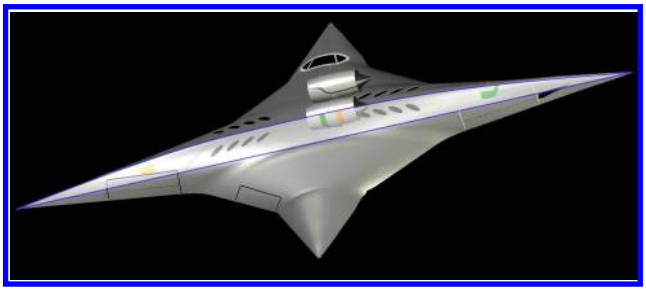

Figure 4: A SBiDir-FW civil transport in supersonic mode flying toward right, supersonic thin airfoil highlighted in the middle.

For a SBiDir-FW configuration, usually the maximum cross section area is at the wing span location at 50% of the airplane length. A_{max} and V may be evaluated as the following:

$$A_{max} = b * t_{avg_b}, \quad V = S * t_{avg_{all}} \tag{4}$$

where t_{avg_b} is the averaged thickness at the wing span location, $t_{avg_{all}}$ is the averaged thickness of the whole airplane.

$$C_s = S/b^2(\frac{t_{avg_{all}}}{t_{avg_b}}) = \frac{t_R}{AR}, \quad t_R = \frac{t_{avg_{all}}}{t_{avg_b}} \tag{5}$$

where t_R is the averaged thickness ratio of the overall airplane to the one at span location. Once the thickness of the configuration is chosen, the slenderness is determined by the planform aspect ratio. The smaller the aspect ratio, the higher the slenderness coefficient.

For the same sweep angle, planform area, and thickness distribution, a diamond wing as sketched in Fig. 4 will have an aspect ratio half of a delta wing, which represents a wing planform of a conventional wing-tube configuration. A diamond wing will have the length $\sqrt{2}$ (1.414) time longer than that of a delta wing and the wing span is $\sqrt{2}/2$ time shorter. Note that this comparison only includes the wing planform. For a SBiDir-FW configuration, the wing planform is the whole airplane. For a conventional wing-tube airplane, the fuselage takes a substantial volume and is also the maximum length. The slenderness coefficient of a SBiDir-FW configuration hence will be more than 2 times greater than that of a conventional wing-body configuration. The lift distribution length of a SBiDir-FW configuration is the whole airplane length from head to tail, the maximum possible length of an airplane. The higher slenderness (smaller aspect ratio) and longer length are all beneficial to reduce shock strength, mitigate coalescing of compression wave in the mid-field, and ultimately minimize the sonic boom and wave drag. Furthermore, the flying wing configuration uses the whole body area as the lifting surface. In other words, it uses the maximum possible length and least possible area, which will satisfy the required volume of the mission with minimum weight. Attributed to the supersonic flow characteristics that disturbance only travels downstream, a small aspect ratio brings little induced drag penalty that occurs at subsonic.

2.2 Favorable Aspect Ratio at All Speeds

As indicated by Eq. 1 and 5.2, the smaller the supersonic aspect ratio, the higher the subsonic aspect ratio; the larger the supersonic sweep angle, the smaller the subsonic sweep angle. The conflict of subsonic and supersonic aerodynamic performance of conventional tube-wing configuration is hence removed by rotating the airplane 90°. In other words, designers can favor the supersonic aerodynamic performance as much as needed and do not have to compromise for subsonic performance. High supersonic aerodynamic performance could be naturally translated to high subsonic performance. Conventional supersonic wing-tube configuration usually do not use aspect ratio smaller than 2. Otherwise, they will have difficulty during takeoff and landing at low speed. For SBiDir-FW, a typical supersonic aspect ratio is about 0.5, which translate to subsonic aspect ratio over 10. As an example of conventional design, the Concorde has excellent supersonic aerodynamic efficiency of L/D=7, but its subsonic L/D is only 4. For SBiDir-FW with high aspect ratio and higher maximum lift coefficient at subsonic, the take-off and landing performance at low speed is outstanding.

2.3 Efficient Use of Area to Reduce Weight

For the SBiDir-FW without a non-lifting fuselage, all area and volume contributes to lifting surface. For the same payload, the overall size of the airplane hence is smaller and lighter. In fact, the supersonic longitudinal symmetric airfoil section, which is equivalent to the "fuselage" of the conventional wing-tube configuration that generates little lift but drag, plays the most important role to produce lift, reduce shock strength, and the associated sonic boom and wave drag. Hence the design philosophy is very different from the conventional design.

2.4 Applicable to Hypersonic Vehicles

The same principle and advantages of SBiDir-FW also apply to hypersonic flight such as one-stage to orbit reusable vehicles to have low wave drag at hypersonic and high lift and controllability at take off/landing at regular airports.

3 Geometry Model

A geometry model is crucial to provide the required controllability to achieve the aerodynamic performance, specifically to minimize shock strength in this research. An ideal geometry model will allow designers to explore the design space with minimal design parameters to achieve the optimum design either manually or using automated design optimization. In this research, an advanced geometry model for this purpose is developed following the strategy for transonic and supersonic aircraft engine compressor/fan blades[23].

The wing is created by stacking a series of airfoil along leading edge. In our designs, we use 5 to 8 airfoil sections to form a flying wing. A leading edge sweep and dihedral angle distribution can be specified at any leading edge point. Once the sweep and dihedral angle distribution are determined, the flying wing planform is determined, so are the planform area and aspect ratio. Since a SBiDir-FW has a symmetric planform, the airfoil needs to be symmetric about the 50% chord location. Hence the maximum thickness location is at 50% of the chord. After the planform

is determined, the next most important step is to generate the meanline angle distribution of each airfoil.

Once the meanline angle is determined, the actual meanline curves are generated by using a spline technique. Then the airfoil is formed by adding the thickness circles along the airfoil meanlines. Again, due to the symmetric requirement, the meanline angle distribution is symmetric about 50% chord location. Our geometry model allows designers freely adjust the meanline angel distribution of each airfoil. The meanline angle is to control the incidence angle of the flow approaching the airfoil, the total flow turning that controls the aifoil loading, and local flow turning that control the local expansion and shock waves.

The definition of flow incidence is similar to angle of attack of an airfoil, but not the same. The flow is defined as the angle between the flow velocity vector and the meanline angle at leading edge. If the flow velocity has the same direction as the airfoil meanline angle, the incidence is zero. If the flow angle is greater than the LE meanline angle, the incidence is positive, otherwise, the incidence is negative. For a supersonic thin airfoil, a zero incidence will generate a weak LE shock since the flow is aligned with the LE. A positive incidence is expected to generated a stronger LE shock going downward and a local expansion on the suction surface LE region. A negative incidence would be opposite to generate a stronger shock going upward and a local expansion on the pressure surface LE region.

The airfoil thickness distribution from the leading edge to the maximum thickness is determined following a quarter-sine wave distribution. For leading and trailing edge, the designers also need to specify the thickness. An ellipse at leading edge(LE) and trailing edge (TE) will then be formed based on the thickness and the ratio of the major and minor axes ratio. A graphical user interface (GUI) is developed using Java language to allow designers directly adjust the meanline angle distributions point by point using mouse click. The meanline angle distribution adjustment is based on the airfoil surface isentropic Mach number distributions predicted by CFD, which indicates the flow incidence, shock location, and shock strength. The principle is to give the airfoil a moderate incidence to weaken the front shock and a favorable turning on the airfoil to minimize the shock strength. How to create desirable meanline angle distributions for each airfoil section to minimize the sonic boom and maximize ratio of lift to drag is the critical part of the design, which will be elaborated more in the later section when we explain the designs achieved. The designers can instantly see the airfoil shape change on the screen when they vary the meanline angle distribution of each airfoil using the GUI.

4 Numerical Approach

The in house high order accuracy CFD code FASIP, which is intensively validated with various 2D and 3D steady and unsteady flows including sonic boom[24, 25, 26, 27, 28], is used for the CFD analysis. To accurately capture shock waves and sonic boom, high order shock capturing schemes, including 3rd order MUSCL scheme[29], 3rd, 5th and 7th order WENO schemes and a finite compact scheme combining a shock detector and 6th order Pade scheme, are utilized in the code[26, 27, 28, 30]. A set of 4th order and 6th order central differencing schemes are devised to match the same stencil width of the WENO schemes for the viscous terms[31, 32]. The Roe's scheme [33] and a low diffusion E-CUSP scheme developed by Zha et al[34] are used as the approximate Riemann solver with the MUSCL and WENO shock capturing schemes. For turbulent simulations, FASIP has implemented Detached Eddy Sim-

ulation (DES)[35, 36, 37, 38, 39, 40, 41], Large Eddy Simulation(LES)[32, 42], and Reynolds averaged Navier-Stokes (RANS)[43, 31, 44, 45, 46, 47, 48, 49]. An implicit 2nd order time accurate scheme with pseudo time and unfactored Gauss-Seidel line relaxation is employed for time marching. For aeroelasticity problems, a fully coupled fluid-structural interaction model is implemented[50, 41, 49, 37, 43, 45, 46, 36]. The MPI parallel computing is utilized and a high scalability is achieved[51].

The Euler inviscid solver using the high resolution 3rd order weighted essentially non-oscillatory (WENO) scheme with Roe's approximate Riemann solver, which is validated with accurate prediction of sonic boom, is used for design iterations at supersonic mode. The Euler solver also predicts lift and pressure drag accurately. The only drag missing from an Euler solver is the supersonic surface friction drag. Winter and Smith [52] conducted rigorous experimental study of supersonic friction drag for delta wings, which has the airfoil maximum thickness of 8.3%, Mach number from 1.5 to 2.6 and angle of attack (AoA0 up to 10°. The delta wing is tappered and twisted. His conclusion is that despite the wide variations in skin friction on the wing surface, the total skin-friction drag is probably only some 5 to 10 per cent less than that on a flat plate due to the adverse pressure gradient. The drag shows little variation with incidence.

Since the SBiDir-FW configurations simulated in this initial research do not include the propulsion systems, and the ranges of Mach number, sweep angle, AoA and airfoil thickness are all within the same range of Winter- Smith experiment[52], we hence adopt the flat plate surface friction coefficient modified for different altitude as the surface friction coefficient of SBiDir, which is on the conservative side of the drag estimate. The utilization of flat plate surface friction coefficient for SBiDir-FW design iteration not only saves tremendous CPU time of CFD simulation, it is also more reliable than the friction prediction from Reynolds averaged Navier-Stokes (RANS) solvers[53], which often have difficulty in accurately predicting drag. The same way using flat plate friction coefficient for supersonic wing is also adopted by Seebass[54].

The viscous Navier-Stokes solver is used to predict the lift, drag (with both pressure and friction drag) and moments for the subsonic mode of SBiDir-FW, which has thick airfoil and flow separation. A flat plate friction coefficient would not be as accurate as for supersonic mode with thickness less than 3% and no flow separation.

In most of the trade studies, the far field sonic boom propagation to ground is simulated using the the NASA *NF Boom* code[55]. In the final study with refined mesh to be presented in Section 6, the sBOOM code recently developed in NASA with non-linearity, molecular relaxation and thermo-viscous absorption[] is utilized.

4.1 Mission Requirement

To implement realistic constraints for this conceptual design using SBiDir-FW, the mission requirement include cruise Mach number of 1.6, pay load of 100 passenger with standard luggage, and range of 4000nm. The text book *Design of Aircraft* by Corke [56] provides an excellent aircraft conceptual design methodology, which is adopted for the SBiDir design. A FORTRAN code was written based on this methodology in order to facilitate the design iterations.

To maximize the benefit of SBiDir-FW concept, a length of 100m is selected so that we can use thin airfoil with the thickness less than 3%, which will give sufficient headroom space and volume to hold passengers and fuel. It turns out that the volume is in general easy to achieve due to the inherent advantage of flying wing. Once the sweep and dihedral angles distributions are specified,

the planform area is determined. When the complete SBIDir-FW geometry is determined and CFD analysis is completed, the coefficients of lift, drag, moment and the ratio of lift to drag are available. With all these geometry and aerodynamic performance parameters including engine fuel consumption, structure factor, and flight altitude as the input to the mission analysis code, an estimate of the aircraft weight at different flight stages is iterated by using standard estimates of the weight of passengers and crew, luggage, cockpit, engines, and other components. The range is one of the output results from the mission analysis.

In this design, the SBiDir configuration is expected to provide a very low wing loading, and thus short take-off and landing distances are expected. To choose the propulsion system, a computation of the overall aircraft drag is performed to ensure that the plane has sufficient thrust, and then engines that meet the thrust requirements are sized based on a reference engine.

5 Trade Study

To reduce the CPU simulation time, most of the trade studies use coarse meshes of about 3.3 million to see the trend. The final design iterations uses refined mesh of 10.3 million to ensure that high resolution of shock location and strength are resolved. All the meshes have local refinement around the shock to capture the correct shock profile. In other words, the sonic boom value of the trade study may not be reliable due to the coarse mesh used, but the trend is correct. The aerodynamic lift and drag from the coarse meshes are accurate and have little difference from the refined mesh. The optimum design from the trade study is analyzed using refine mesh and is presented in Section 6, which gives reliable ground pressure signature and noise level.

5.1 Mesh

Since SBiDir-FW is symmetric about mid-span, only half of the airplane is simulated with symmetric boundary condition used at mid-span plane. The mesh is constructed using the H-mesh topology in order to achieve high quality around the sharp LE and TE of the airfoils. The coarse mesh displayed Fig. 5 uses a total of 251 points in the streamwise direction, 81 in the spanwise direction, and 161 points in the direction normal to the wing surface. Total coarse mesh size is 3.27 million points, partitioned into 40 blocks for the parallel computation. A refined grid is constructed using 1.5 time more points in each direction with the total grid points of 10.3 million.

A large amount of trade studies are carried out. The following sections only show some of them to demonstrate the features of SBiDir-FW concept.

5.2 Sweep and Dihedral Angle

The sweep angle needs to be determined first to form the planform shape, which decides the aspect ratio at supersonic and subsonic. Aspect ratio is critical to determine the lift, drag, and aerodynamic efficiency of L/D. For supersonic flight, a high sweep angle is always desirable since it generates low shock strength, sonic boom, and wave drag. As an example of extreme, a sweep angle of 89° will be basically a 2D airfoil slice with tiny span width and will generate acoustic

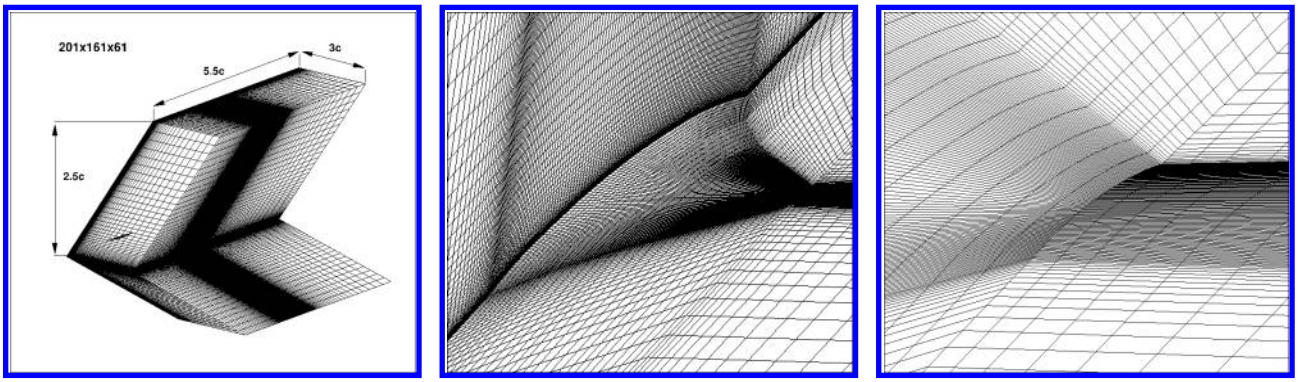

Figure 5: SBiDir mesh topology, outside mesh (left), suction surface (middle) and wing tip (right).

wave with no sonic boom. However, it is useless since there is no volume to hold passengers and fuel. In general, decreasing the sweep angle within the Mach cone will increase supersonic aspect ratio, planform area, volume, lift, wave drag, ratio of lift to drag, shock wave strength, and sonic boom. To satisfy the mission requirement, a high L/D and sufficient lift coefficient is required, and a lower sweep angle is preferred. However, a lower sweep angle will increase the aspect ratio, make the planform less slender, and increase sonic boom. In simple words, a very slim planform is beneficial to reduce sonic boom, but being too slim will not have enough lift and volume to fly the mission. So there is a balance between the required aerodynamic performance for the mission target and the low sonic boom goal.

The table in Fig. 6 gives two different sweep angle design examples at the early stage of this research, namely D84TW and D82S4. The two designs have constant sweep angle of 84° and 82° respectively with diamond shape planform.

	General characteristics, M=1.6, L=100m												
Design	Area (m^2)	AR sup	AR sub	Passen-gers	TO weight (klb)	Alt (kft)	Ground Boom (dBPL)	L/D, M>1	L/Dp	CL	L/D, M<1	Range (nm)	Pass*mile/lb fuel
D82S4	706	0.28	14.16	100	191.5	42	81.6	6.48	19.11	0.0363	12.5	3000	3.58
D84TW	528	0.20	18.94	60	110.7	42	63.8	5.50	18.73	0.0296	N/A	2500	3.11

Figure 6: Performance of Design D84TW and D82S4.

Fig. 7 shows the Mach number contours on the suction and pressure surface, which also displays the slim planform shape. Fig. 8 is the Mach number contours at different span, indicates that there is a shock wave going upward on the suction surface and an expansion wave going downward. The airfoil used to stack the wing is simple circular arc airfoil with linear meanline angle distribution. The thickness varies from 2.2% in the 0% span to 0.5% span in the tip. The surface isentropic Mach number distributions at different span shown in Fig. 9 indicates that the region near tip is highly loaded and near center is lightly loaded. A more even loading distribution will be more desirable.

Fig. 10 is the lift and pressure drag coefficient variation with AoA. The lift is almost linearly

increased with increasing AoA. The pressure drag grows slower at low AoA and increases more rapidly at high AoA. The pressure drag is over a order of magnitude smaller than the lift and yields a L/D_p about 19 (Fig.6) at AoA=3°. However, since the surface friction drag primarily depends on Mach number and Reynolds number, the friction drag is more dominant and brings the overall L/D down to about 5.5 as shown in Fig. 7. The volume of D84TW only allows it to carry 60 passenger and the range is 2500nm due to the moderate L/D. The flight altitude is 35kft to gain freestream density to compensate the low lift coefficient.

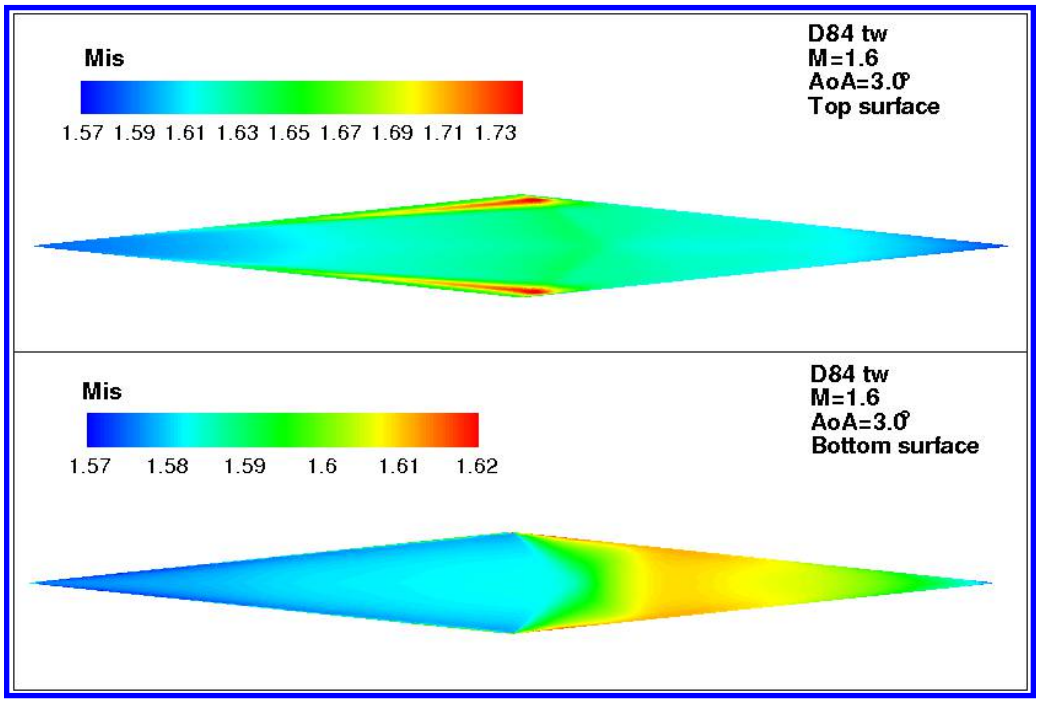

Figure 7: Isentropic Mach number contours of D84TW at AoA=3°, top: suction surface, bottom: pressure surface.

Decreasing the sweep angle to certain extent within the Mach cone will increase aspect ratio, the slope of lift vs AoA, and hence lift coefficient and L/D at the same AoA. Since the D84TW's lift coefficient and L/D are not sufficient to carry 100 passengers for the range of 4000nm, a design with sweep angle of 82°, D82S4, is conducted.

As shown by Fig. 6, decreasing the sweep angle by 2° from 84°, the aspect ratio is increased by 40% from 0.2 to 0.28, the planform area increased by 34%. At the same AoA=3°, the lift coefficient is increased by 23%, L/D increased by 18%. The volume increase is sufficient to carry 100 passengers with the range increased to 3000nm. Even though the ground boom signature shape is still *Sine* shape wave. The ground boom loudness is increased to 81PLdB from flight altitude of 42kft. In general, a low sweep angle will give better L/D, but stronger sonic boom.

To further increase L/D without considering much the sonic boom, a variable sweep is more beneficial to have lower boom and low wave drag as shown by design D84-68.11 in Fig. 11, which has a variable sweep distribution from 84° at the very leading edge to 78° at the wing tip. The supersonic aspect ratio is increased to 0.632 with the lift coefficient of 0.086 as shown in Table 1. The L/D is very high up to 10.45. Due to the increased L/D, volume, and planform area, this airplane can carry 200 passengers for 5000nm at altitude of 56kft with a strong ground sonic boom loudness of 101.64PLdB and a N-wave.

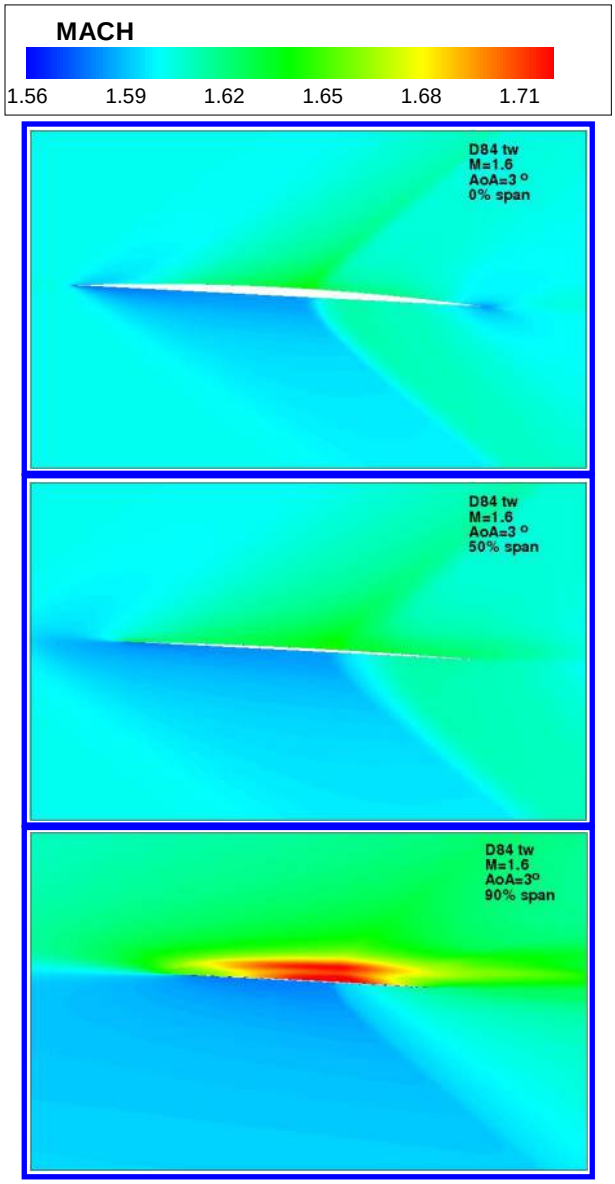

Figure 8: Isentropic Mach number contours of D84TW at different span location, AoA=3°.

Due to the time limitation, no optimization of sweep angle is conducted. This trade study is to understand the sensitivity of sweep angle to the aerodynamic and sonic boom performance. The general conclusion is that a lower sweep angle will give high L/D and high sonic boom. The L/D of 10.45 and the sonic boom achieved in this study still has a lot of room to go and is definitely not the limit. More effort to improve this design will be continued. An optimal sweep angle distribution needs to be studied next step.

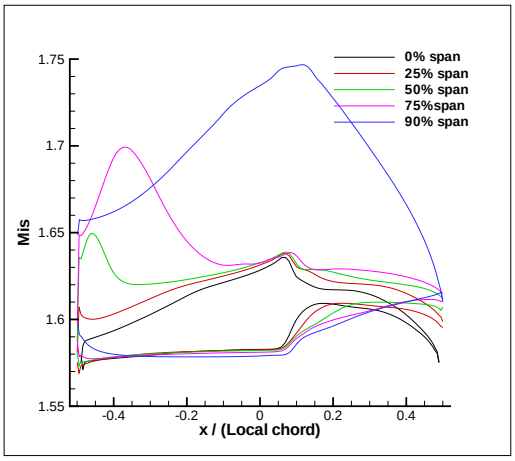

Figure 9: D84TW surface isentropic Mach number distributions.

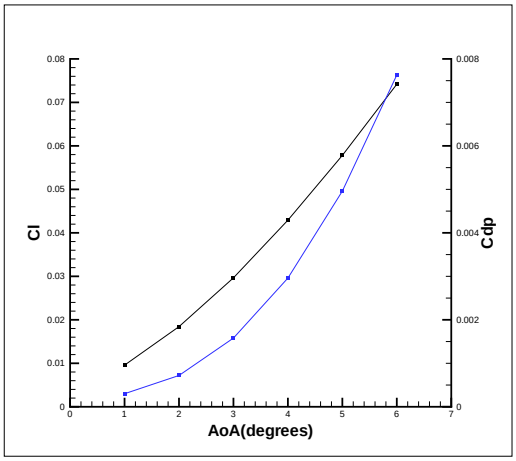

Figure 10: D84TW lift and drag coefficient vs angle of attack.

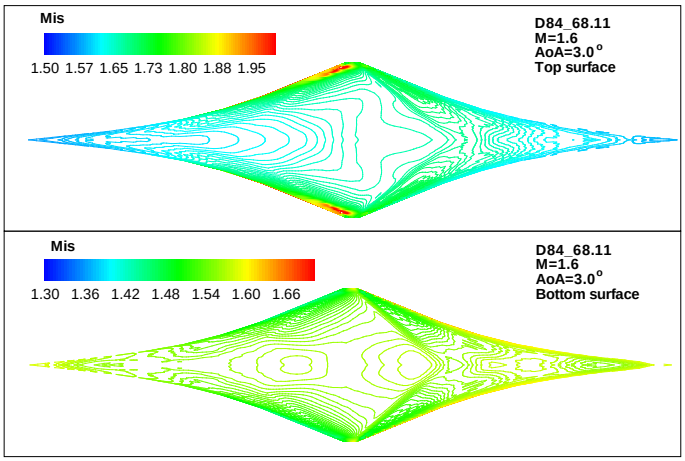

Figure 11: Isentropic Mach number contours of D84-68 at AoA=3°

Table 1: Geometry information

Length(m)	Span(m)	Area(m^2)	Volume(m^3)	AR(subsonic)	AR(supersonic)
100	23.7	891	585	11.23	0.632
Cl	Cd	Cl/Cd			
0.08613	0.00824	10.453			
Altitude(ft)	30000	40000	50000	56000	
Noise(PLdB)	111.12	106.38	101.64	99.08	

5.3 Meanline Angle Distribution

To further reduce sonic boom with increased L/D, the meanline angle distribution is found to be the most effective way to control shock strength. The meanline angle distribution can be varied for each airfoil section to adjust the flow incidence at leading edge, control the loading distribution along the chord, and hence control the shock strength. The basic strategy is to minimize the surface shock strength in order to provide a favorable near field over-pressure signature, which will further reduce the ground sonic boom level. The total meanline angle variation from LE to TE stands for how much the flow is turned by the airfoil, which determines the total lift or loading of the airfoil.

In this study, all other design parameters including sweep angles, dihedral angles, airfoil thickness, leading edge (LE) and trailing edge (TE) thickness are held unchanged. A variable sweep from 84° to 78° is adopted to increase the aspect ratio to 0.355 in order to further increase L/D up to 8.4. Again, many design trails are conducted and only three of them are presented in this section to demonstrate the effect.

As comparison, Fig. 12 presents three different meanline angle distributions at different span locations. The zero span meanline angle is found to have the most impact on the sonic boom due to its longest chord length in the flying wing planform. The discussion in this subsection is hence mostly on the zero span airfoil. All meanline angle distributions are symmetric about the 50% chord location to ensure the symmetry requirement of SBiDir-FW concept.

The left plot in Fig. 12 is a linear distribution from LE to TE, which represents a circular arc airfoil. For an ideal 2D supersonic flow, a linear meanline angle distribution means the flow on the suction surface will have uniform expansion from LE to TE, and the flow on pressure surface will have uniform compression. For 3D wing with high sweep angle, the flow has some similar feature, but is altered significantly since the flow pressure needs to return to ambient pressure after TE.

The middle plot in Fig. 12 has a nonlinear distribution with half of the total turning imposed on the first 25% of the chord, almost no turning from 25% to 75% chord, and another half turning imposed at the last 25% chord due to the symmetry requirement of the airfoil geometry. Removing the flow turning in the chord of 25-75% is to weaken the suction surface shock strength by reducing the peak Mach number. Even though the middle plot has nonlinear loading distribution, the turning is reduced monotonically from LE to TE. The right plot in Fig. 12 also has nonlinear distribution similar to the middle plot, but with more enhanced turning effect in the first and last 25% of chord that the meanline angle distribution becomes non-monotonic. The flow turning from 25-75% is actually increasing and creates the reversed cambering. Similar to the zero turning meanline angle distribution in the middle plot, the reversed cambering is to further enhance the peak Mach number reduction by mitigating the expansion on suction surface. Such non-monotonic meanline angle distribution is successfully applied to remove shock waves for a transonic compressor blade with supersonic inlet Mach number by Hu et al[23].

Fig. 13 is the comparison of surface isentropic Mach number distribution at different span, the black line is for the linear meanline angle, red for the monotonic, and blue for the non-monotonic. The typical surface isentropic Mach number distribution on the suction surface and pressure surface appears to be fairly symmetric as shown by the linear distribution case(black line). That is, while the flow on the suction surface expands and accelerates , the flow on the pressure surface is compressed and decelerates. They reach the highest and lowest peak at the same location. Then the flow on suction surface goes through a shock wave and the flow on

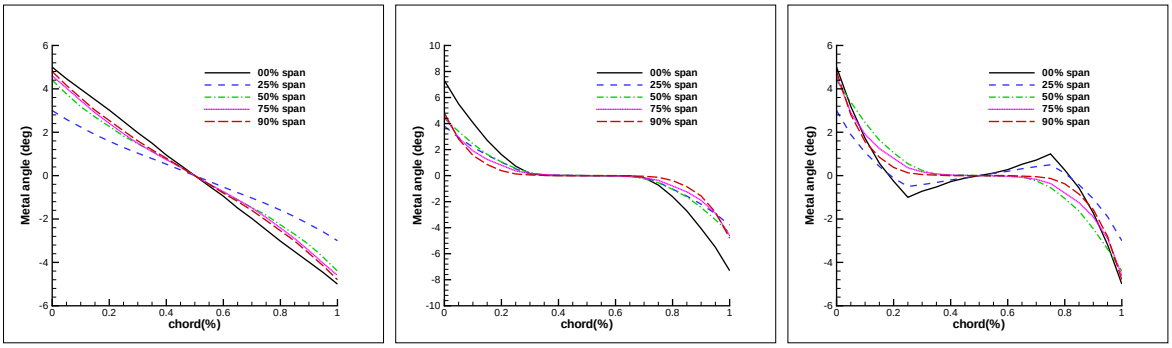

Figure 12: Three different meanline angle distributions, left: linear; middle: monotonic; right: non-monotonic.

pressure surface goes through a rapid expansion wave. The flow on suction and pressure surface meets the ambient pressure at the trailing edge.

Changing the meanline angle distribution from the linear to the monotonic (red line) drastically changes the loading distribution, which is more uniform from LE to TE along the chord. The strength of shock wave on suction surface and expansion wave on pressure surface are significantly reduced. The non-monotonic meanline angle distribution(blue line) further reduces the peak Mach number compared with the monotonic one. The non-monotonic distribution has the same LE meanline angle as the linear one, but the flow incidence is less due to the rapid decrease of the meanline angle after the LE. The more important effect is that the high peak Mach number on suction surface is reduced and the low peak Mach number on pressure surface is increased. In other words, the shock wave on suction surface and expansion wave on pressure surface are both reduced. Such effect is maintained in most of the span until near tip, where the linear meanline angle distribution has lower peak Mach number. Applying linear meanline angle distribution near tip is hence expected to further improve the results. Table 2 to 4 summarize the performance of the three designs. Compared with the linear meanline angle distribution, the non-monotonic one reduces the lift by 10%, but gain the L/D by 3% with the value of 8.4 due to reduced wave drag by weaking the shock waves.

Fig. 14 compares the suction and pressure surface Mach number contours of the linear and non-monotonic meanline angle distribution with the exact same planform shape determined by the variable sweep. For the linear one on the left, there is a strong shock wave on the suction surface emanating from the tip. At the same location on the pressure surface, there is a strong expansion wave. The shock wave on the suction surface and the expansion wave on the pressure surface always go hand in hand to balance the pressure. For the non-monotonic one on the right, both the shock wave and expansion wave are significantly weakened.

Fig. 15 displays the Mach contours at different span showing the wave structures propagating in the near field. The front 60% of the airplane generates the compression wave propagating downward and expansion wave travling upward. Even though the non-monotonic meanline angle design has almost no strong waves on the wing surface, there is still an oblique shock formed on upper surface going upward and an expansion wave propagating downward because the flow has to match the pressure of ambient.

Such a wave pattern is determined by the lift requirement. In other words, as long as an object generates lift regardless of the specific configuration, the wave propagating downward will have compression in front, followed by an expansion, and end with an aft compression wave to

return the flow pressure to ambient. The hope is not to let the compression in the front and aft coalesce into two shock waves in order to avoid the N-wave, which has sharp pressure rise within a very short time that generates strong noise and annoyance. It is hence beneficial to let the compression occurs in a longer distance in a more graduate way to have less compression coalesce in far field. The high slenderness of SBiDir-FW provides an advantage to prolong the compression and expansion with smaller slope. The mitigation of strong shock wave on suction surface and compression wave on pressure surface is to achieve a graduate variation.

The most important benefit of changing the meanline angle distribution from linear to nonlinear and non-monotonic is it drastically reduces the ground sonic boom noise. Fig. 16 shows the over pressure signature at 2-body below and the propagation to ground. The nonlinear meanline angle distribution has a much lower compression and expansion peak than the linear one in the near field and the pattern is maintained to far field. However, the linear design's high compression peak coalesce to a strong shock in the far field, whereas the nonlinear one remain as smooth wave. Table 2 to 4 indicates that the nonlinear meanline angle distributions reduce the ground boom loudness by as much as 24-25PLdB at the flight altitude of 56kft from the linear design of 91PLdB to 67-66PLdB. At the same time, the planform shape is unchanged and the L/D is increased by 3% to 8.4.

The most important and encouraging finding from this meanline angle distribution study is the qualitative trend instead of the quantitative values, which need to be confirmed by refined mesh, wind tunnel experiment and eventually flight testing. This qualitative direction establishes an effective control relationship between the far field ground sonic boom with the aircraft geometry parameters based on a clear aerodynamic physics principle, which is to generate the loading distribution along a slender body with as smooth distribution as possible without strong shock and expansion waves. An optimal design can be eventually achieved with detailed efforts such as design optimization under an effective qualitative guideline.

Table 2: Linear meanline angle distribution

Length(m)	Span(m)	Area(m^2)	Volume(m^3)	AR(subsonic)	AR(supersonic)
100	15.7	690	462	14.492	0.355
Cl	Cd	Cl/Cd			
0.06284	0.00762	8.14			
Altitude(ft)	36000	40000	50000	56000	60000
Noise(PLdB)	99.68	98.45	95.28	91.14	88.38

Table 3: Monotonic meanline angle distribution

Length(m)	Span(m)	Area(m^2)	Volume(m^3)	AR(subsonic)	AR(supersonic)
100	15.7	690	544	14.492	0.355
Cl	Cd	Cl/Cd			
0.05810	0.00698	8.324			
Altitude(ft)	36000	40000	50000	56000	60000
Noise(PLdB)	72.40	71.75	68.85	67.28	66.16

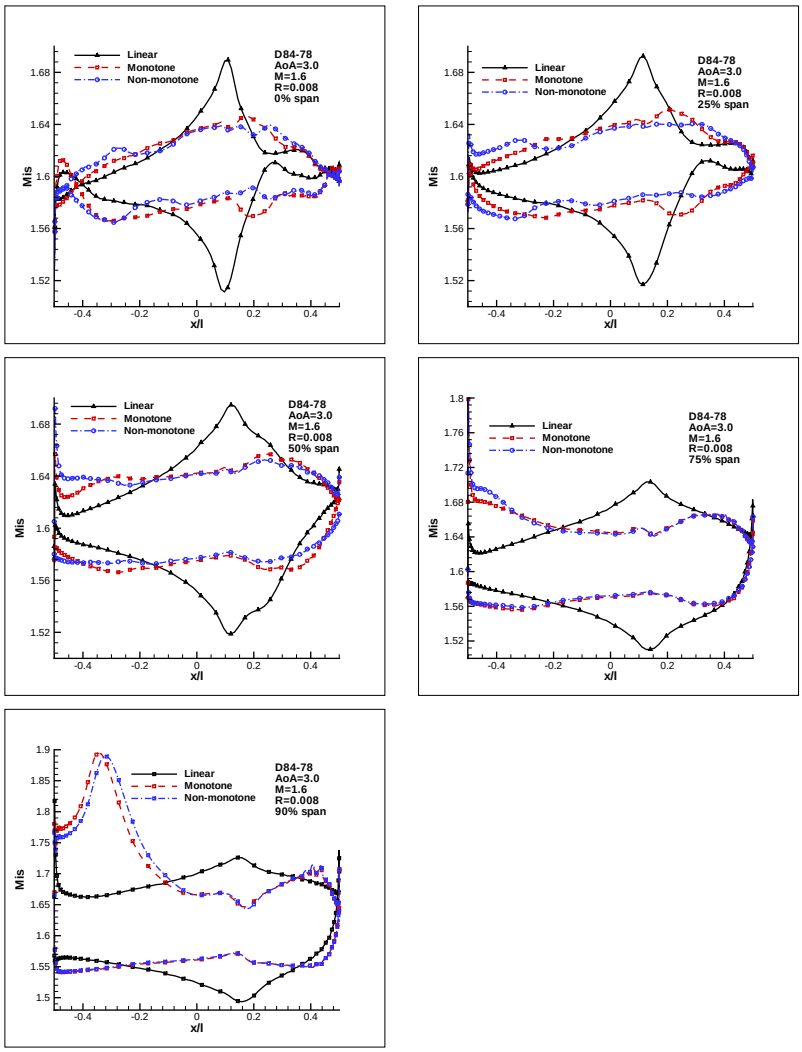

Figure 13: Wall Isentropic Mach numbers distribution along the chord at different spans.

Table 4: Non-Monotonic meanline angle distribution

Length(m)	Span(m)	Area(m^2)	Volume(m^3)	AR(subsonic)	AR(supersonic)
100	15.7	690	511	14.492	0.355
Cl	Cd	Cl/Cd			
0.05628	0.00671	8.3875			
Altitude(ft)	36000	40000	50000	56000	60000
Noise(PLdB)	71.12	70.70	67.99	66.41	65.41

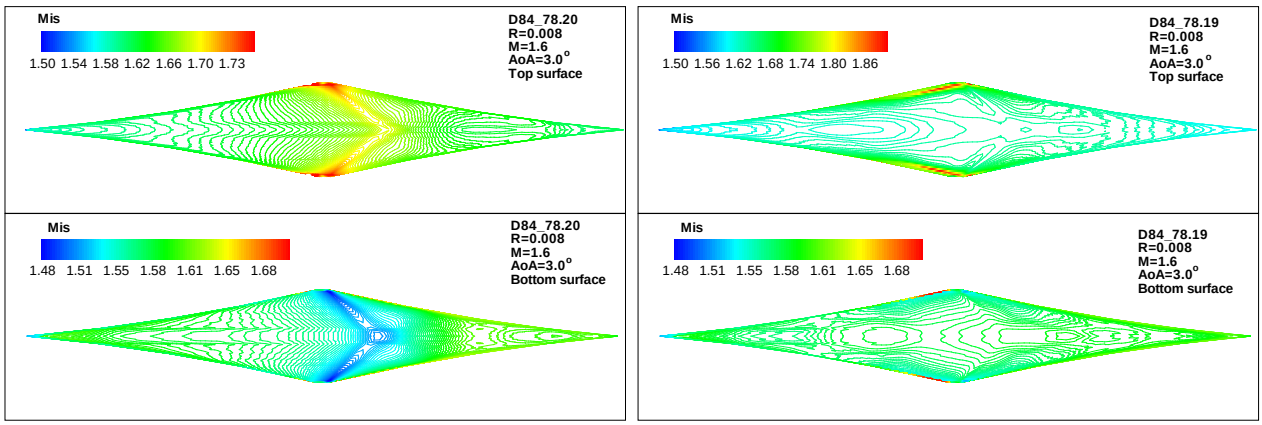

Figure 14: Comparison of surface Mach number contours. Left: linear; Right: Non-monotonic

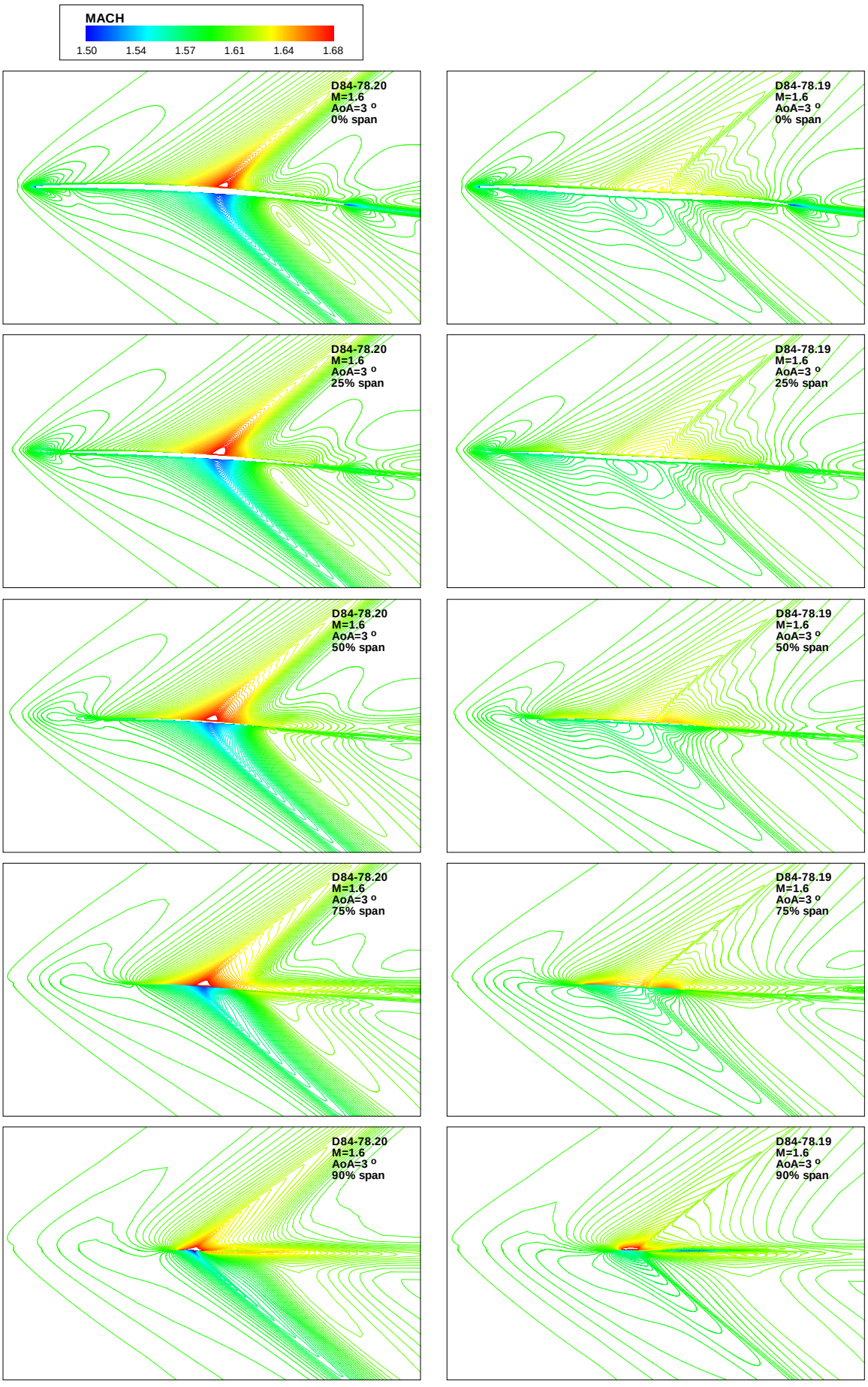

Figure 15: Comparison of Mach number contours at different spans

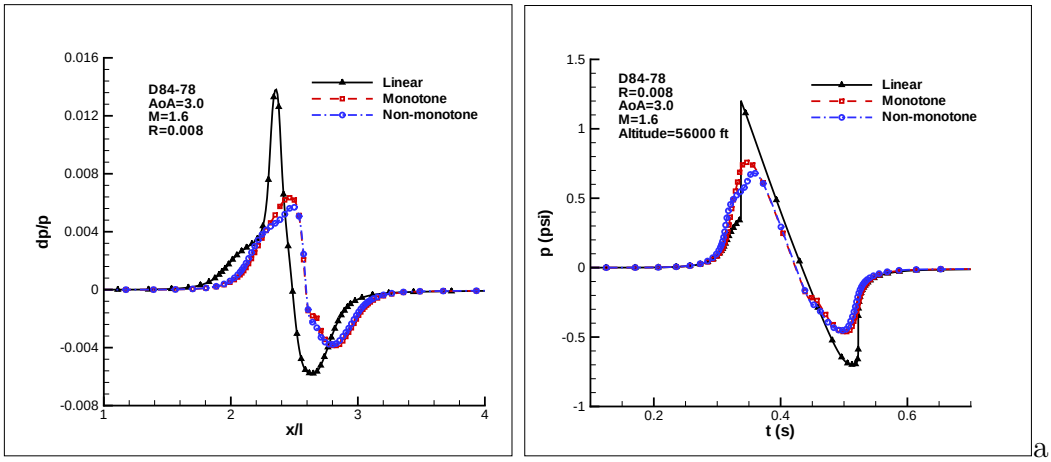

a

Figure 16: Comparison of overpressure signature. Left: 2 body length below; Right: ground sonic boom signature

5.4 Angle of Attack

The same design D84-78.19 analyzed in above section 5.3, which has the meanline angle distributions tailored for AoA=3° to weaken the surface shock wave, is conducted for trade study with AoA 1°, 2° and 4° to see their aerodynamic and sonic boom performance. Table 5, 6, and 7 summary the results, which can be compared with the results of D84-78.19 in Table 4.

Table 5 indicates that reducing the AoA to 1° decrease the L/D as expected. Fig. 18 displays the surface isentropic Mach number distributions at different span location for each AoA. At AoA=1°, the closed LE shape of the Mach number distribution at 0% span shows that the flow has a negative incidence at that location as expected. The meanline angle producing fairly smooth surface isentropic Mach number distributions at AoA=3° does generate a shock wave on the suction surface at about 60% chord location and a strong expansion wave on the pressure surface at the same location. Such a wave structure produces a stronger ground sonic boom than at AoA=3° even though the lift at AoA=1° is lower. When the AoA is increased to 2° from 1°, the lift and L/D are increased and the sonic boom is reduced since the Mach number distribution is closer to AoA = 3°, but the boom strength is still slightly higher than the AoA=3°. When the AoA is increased to 4°, the increased incidence generates a strong leading edge downward shock that increases the boom strength. In other words, when the AoA is off the designed value, the sonic boom increases even when the AoA is reduced with the lift coefficient.

Fig. 19 and 20 are the over-pressure signature 2-body below and its propagation to ground. Again, the near field shape is well preserved. Interestingly, the AoA=1° has the lowest wave peak, but not the least boom loudness due to the small shock wave interrupting the expansion and generates a higher noise level than that at AoA=3°, which has a higher wave peak but a smoother wave.

As aforementioned that lifting body will necessarily generate a wave signature with a compression in front, followed by an expansion, and ended with another compression. In general, the higher the lift, the higher the wave peak. This study gives an important conclusion that a higher lift at higher AoA with higher peak does not necessarily generates a louder sonic boom. If the higher peak wave is smoother with longer pressure rising time, the noise could be weaker as the case of AoA=3° compared to AoA=1°.

Fig. 21 shows the Mach number contours at different span locations for different AoA. At zero span, the overall upward shock on suction surface and downward expansion on pressure surface for the AoA=1° is weaker than the one of AoA=3°. However, on the wall surface, the AoA=1° has a stronger root of the waves than the AoA=3° case, which generates a weaker ground sonic boom loudness.

Table 5: AoA=1°

Length(m)	Span(m)	Area(m^2)	Volume(m^3)	AR(subsonic)	AR(supersonic)
100	15.7	690	462	14.492	0.355
Cl	Cd	Cl/Cd			
0.02602	0.00448	5.808			
Altitude(ft)	36000	40000	50000	56000	60000
Noise(PLdB)	76.88	76.64	74.73	73.41	72.44

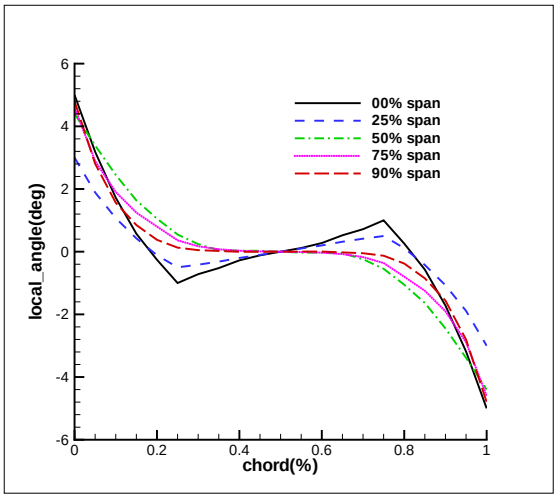

Figure 17: Meanline angle distribution.

Table 6: AoA=2°

Length(m)	Span(m)	Area(m^2)	Volume(m^3)	AR(subsonic)	AR(supersonic)
100	15.7	690	511	14.492	0.355
Cl	Cd	Cl/Cd			
0.03994	0.00529	7.55			
Altitude(ft)	36000	40000	50000	56000	60000
Noise(PLdB)	73.62	72.96	70.24	68.69	67.68

Table 7: AoA=4°

Length(m)	Span(m)	Area(m^2)	Volume(m^3)	AR(subsonic)	AR(supersonic)
100	15.7	690	511	14.492	0.355
Cl	Cd	Cl/Cd			
0.07493	0.0089	8.419			
Altitude(ft)	36000	40000	50000	56000	60000
Noise(PLdB)	83.65	84.95	84.87	84.79	84.49

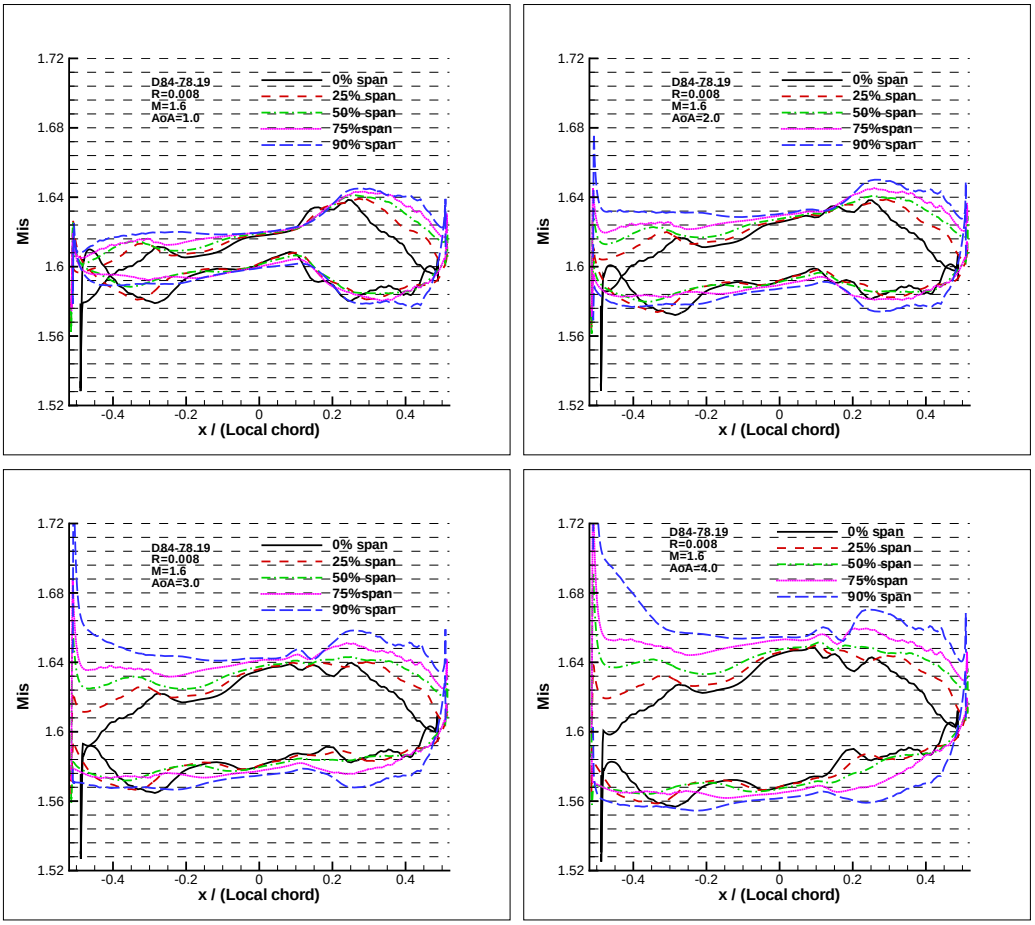

Figure 18: Surface isentropic Mach numbers at different spans for different AoA.

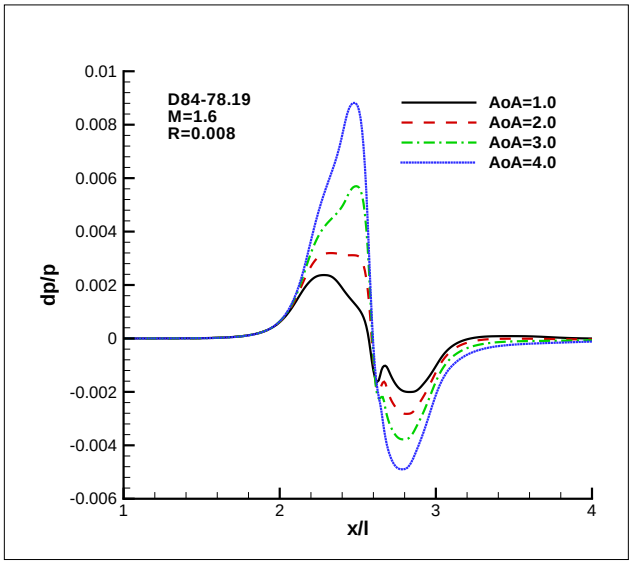

Figure 19: Over-pressure signature 2 body length below at different AoA.

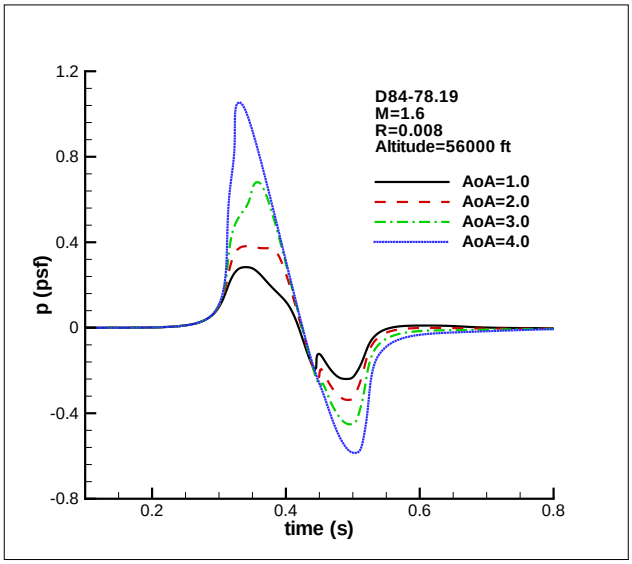

Figure 20: Ground boom signature at different AoA.

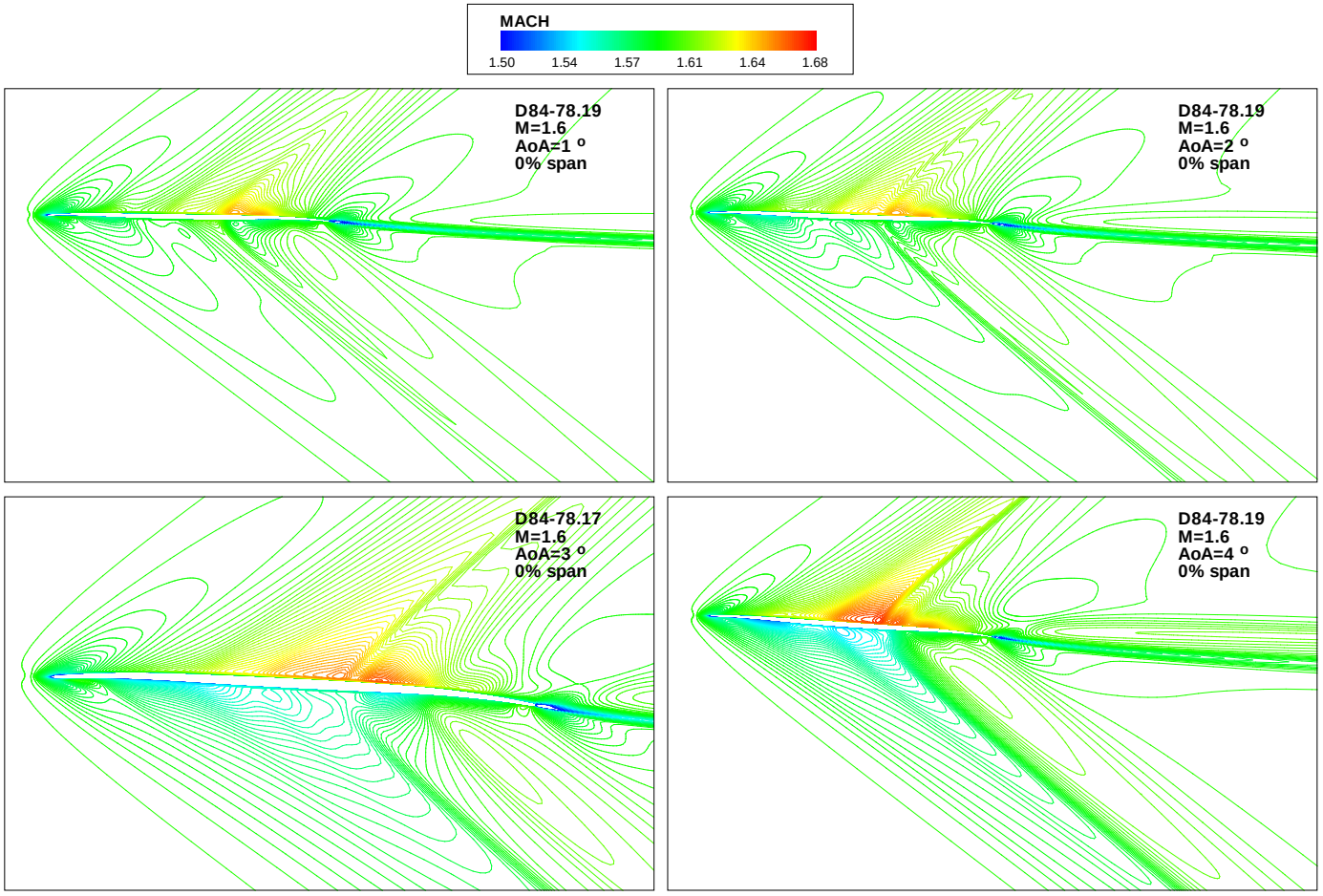

Figure 21: Mach number contours at different AoA

5.5 Leading/Trailing Edge Roundness Study

A sharp leading edge is generally preferred for supersonic airfoil to generate weak attached shock. However, sharp leading edge is difficult to handle variation of AoA. In particular for SBiDir-FW, it needs to fly at subsonic and a round LE is desirable. This trade study is to investigate what influence will a round LE has on sonic boom and aerodynamic performance.

The same design of D84-78.19 studied in section 5.3 and 5.4 is compared with different LE radius from completely sharp ($R_{LE} = 0$) to $d_{LE}/t_{max} = 0.36$ for all the airfoil. For a maximum thickness of 2.2% used in D84-78.19 at zero span, the $d_{LE}/chord$ is about 0.008.

The overall conclusion is that a round LE and TE up to $d_{LE}/t_{max} = 0.36$ has little harm, a small benefit for both sonic boom and aerodynamic performance as demonstrated in Table 8 and 9 with the L/D slightly increased and the sonic boom loudness slightly reduced by 1PLdB.

The more important advantages for using round LE and TE are the following:

1) For the same planform area of the design D84-78.19 , the round LE/TE with $d_{LE}/t_{max} = 0.36$ increases the volume significantly by 18%. This is very important to hold more fuel and payload. Increaseing so much volume without hurting the sonic boom and aerodynamic performance is definitely very desirable. The high sweep angle avoids the penalty that a round LE may create in supersonic flow since the Mach number normal to the LE is subsonc.

2)It significantly increases the AoA range that a SBiDir-FW can operate efficiently and effectively.

Fig. 22 compares the surface isentropic Mach number distributions between the configurations using sharp and round LE/TE with the exact same meanline angle distributions and all other geometry parameters. At zero span, the round LE gives incidence whereas the sharp LE has near zero incidence even though the overall Mach number distribution is similar. The peak Mach number generated by the round LE is also slightly lower. The round LE advantage is more shown for the outer span near tip. The sharp LE generates very high incidence and the round LE accommodate the flow much better with a smaller positive incidence. The peak Mach number generated by the round LE is significantly lower than that of the sharp LE at 90% span.

Table 8: Sharp LE/TE edge

Length(m)	Span(m)	Area(m^2)	Volume(m^3)	AR(subsonic)	AR(supersonic)
100	15.7	690	462	14.492	0.355
Cl	Cd	Cl/Cd			
0.05772	0.00727	7.94			
Altitude(ft)	30000	40000	50000	56000	
Noise(PLdB)	73.67	71.24	68.95	67.57	

Table 9: Round LE and TE with $d_{LE}/t_{max} = 0.36$

Length(m)	Span(m)	Area(m^2)	Volume(m^3)	AR(subsonic)	AR(supersonic)
100	15.7	690	544	14.492	0.355
Cl	Cd	Cl/Cd			
0.05628	0.00671	8.3875			
Altitude(ft)	30000	40000	50000	56000	
Noise(PLdB)	73.63	71.96	67.99	66.41	

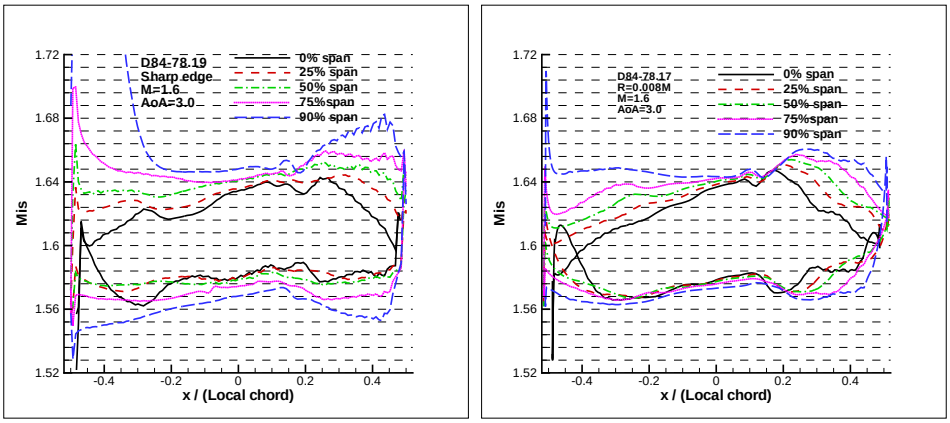

Figure 22: Wall Isentropic Mach numbers at different spans. Left: base design, Right: $d_{LE}/t_{max} = 0.36$

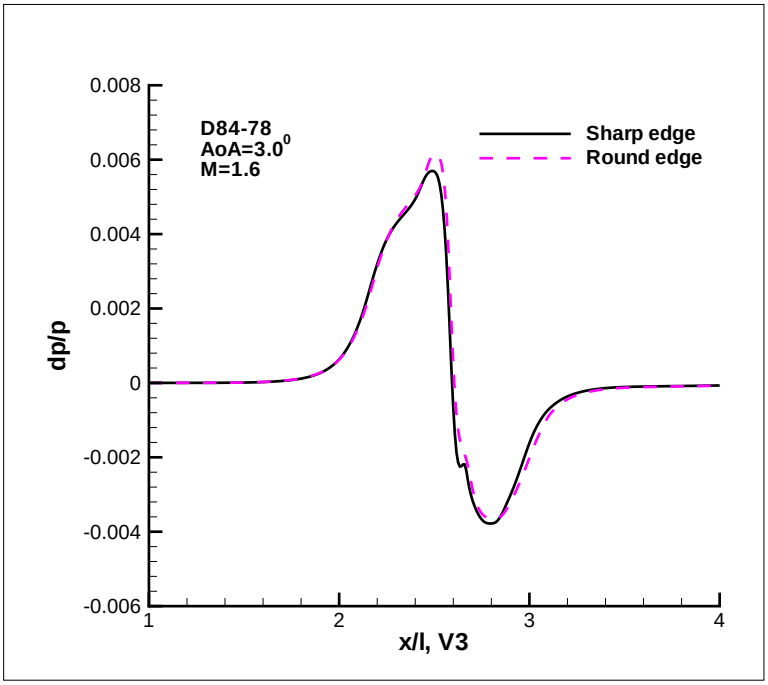

Figure 23: 2 body length below signal

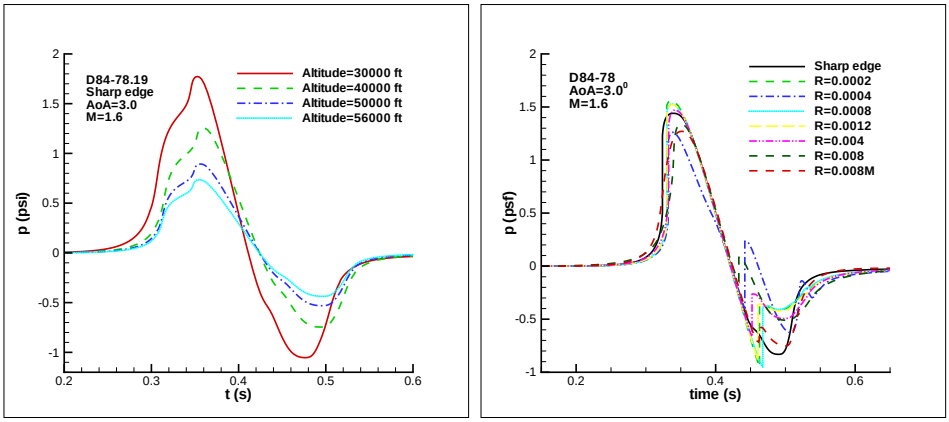

Figure 24: Ground boom(right)

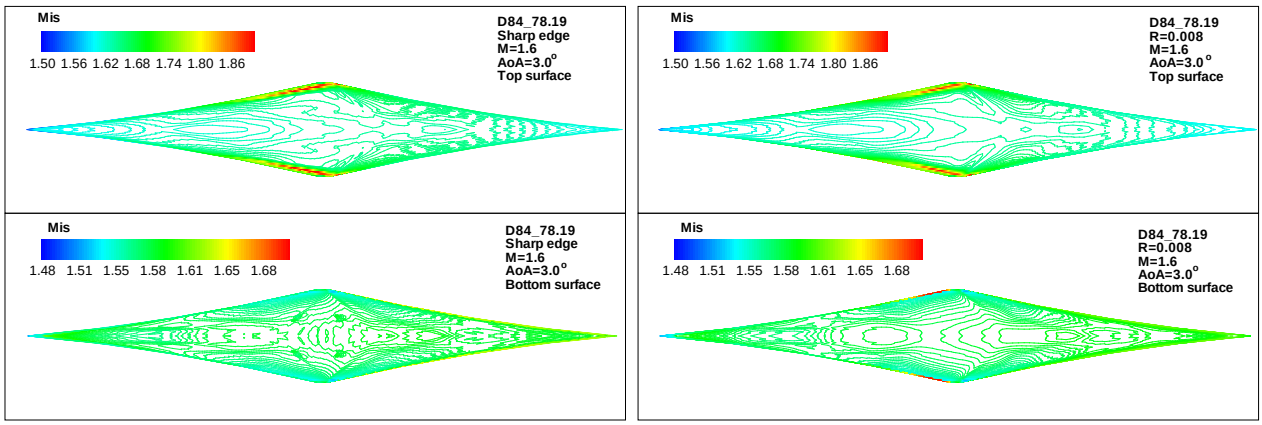

Figure 25: Surface Mach number

6 Optimum Design with Refined Mesh

For SbiDir-FW configuration, the trade studies above demonstrate that both the aerodynamic performance(e.g. CL, CD, Cm) and sonic boom can be directly controlled by smoothing the surface wave distribution using the geometric parameters. However, the sonic boom is much more sensitive to the mesh resolution than the aerodynamic forces. To generate the sonic boom results as accurate as possible, the optimum designs from the trade studies are analyzed using the refined mesh with intensively enhanced resolution in the shock wave regions. The D84-78.39 is the design selected for the final analysis with refined mesh for its excellent overall performance.

Fig. 26 shows the distribution meanline angle of D84-78.39. The non-monotonic meanline angle distribution with reversed camber in the mid-chord region is used within 50% span to mitigate the shock wave strength. The outerspan airfoil mid-chord adopts the near zero turning for the same purpose. The outer span LE meanline angle is about 3° less than the inner span to accommodate the upwash near tip region in supersonic flow. The airfoil thickness in the zero span is 2.2% and is 0.4% at the tip. Fig. 27is the airfoil thickness distribution along the span. Fig. 28 shows the airfoil shapes in different span. The inner span airfoil with reversed cambering can be clearly seen.

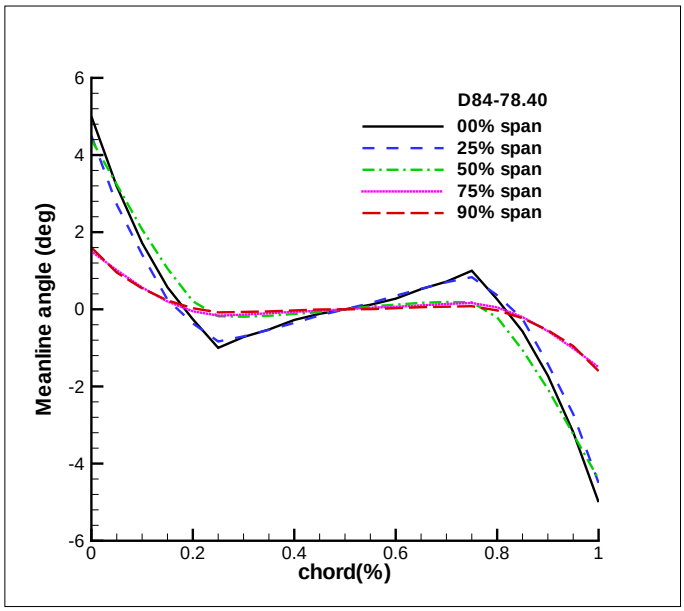

Figure 26: Meanline angle distribution of D84-78.39

The refined mesh has total 72 blocks with 385 points in streamwise, 129 points in spanwise and 197 points in the direction normal to the wing surface, which results in 9.78 million grid points. Fig. 29 and 30 show the zoomed mesh in the zero span plane and on suction surface. The mesh is refined following the shocks waves propagating to far field and along the span.

Fig. 31 is the pressure distribution two body length below the plane, which indicates that the front shock generated from leading edge is very week, virtually a compression isentropic wave. Both the coarse mesh of 3.7million and the refined mesh resolve the front shock wave very well. However, the refined mesh resolves two small shocks during the rapid expansion, which ends up with a very strong shock, much stronger than the coarse mesh predicts.

As another effort to make the ground sonic boom prediction more reliable, the sBOOM [57]

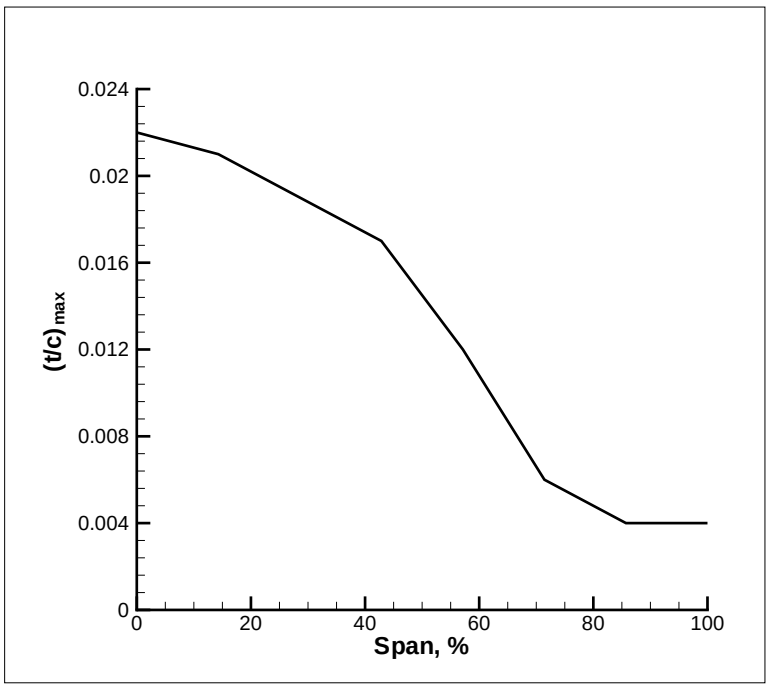

Figure 27: Airfoil maximum thickness distribution along the span.

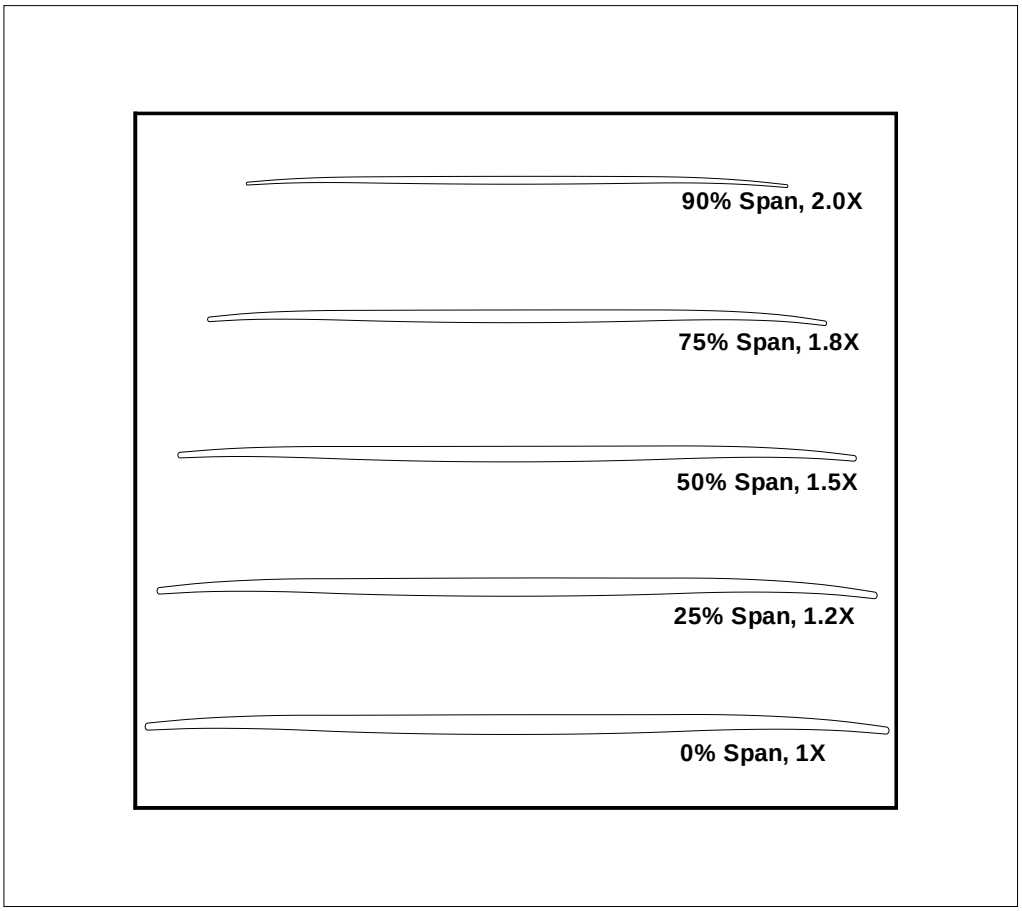

Figure 28: Airfoil shape at different span for Design D84-78.39

code recently developed at NASA is used to predict the pressure wave propagation through atmosphere to ground. Compared with the NASA NFBoom code[55], the sBOOM solves the augmented Burgers equation numerically and takes into account the effects such as non-linearity, molecular relaxation and thermo-viscous absorption into the propagation process. Since the sBOOM has no direct output of the ground sound level in PLdB, the PLdB function in NFBoom is called to obtain the ground perceived level loudness. Since the propagation process is solved numerically in sBOOM, grid convergence test is also conducted. The default number of points used in the wave propagation is 10000. Fig. 32 is the mesh refinement study for sBOOM code, which shows that the ground loudness becomes about constant when the total number of the points is greater than 50,000, which is then adopted in our analysis.

Fig. 33 is the ground sonic boom over-pressure signature for different flight altitude calculated by sBOOM. The front shock remains as a smooth acoustic *Sine* wave shape propagating to ground. The strong rear shock also remains mostly the same shape, but the amplitude is largely dissipated. It makes the rear compression start with a weak shock spike followed by a smooth wave, which increases the rising time and is beneficial to mitigate the sonic boom loudness. No N-shape wave is formed.

Table 10 indicates that the design D84-78.39 achieves L/D of 8.3 and ground sonic boom loudness of 72PLdB at the cruise altitude of 50k ft. This is for the mission of 4000nm, 100 passengers and cruise Mach number 1.6. For this design with its specific over-pressure signature, the ground sonic boom loudness is mitigated with increasing the cruise altitude as shown in Table 10. For the same airplane of 100m length without changing the airplane structure and size, the ground sonic boom loudness will be reduced to 68.4 PLdB and 65.6 PLdB if the airplane flies at 56k ft and 60k ft altitude respectively. Increasing the altitude without changing the design can be achieved by reducing the range.

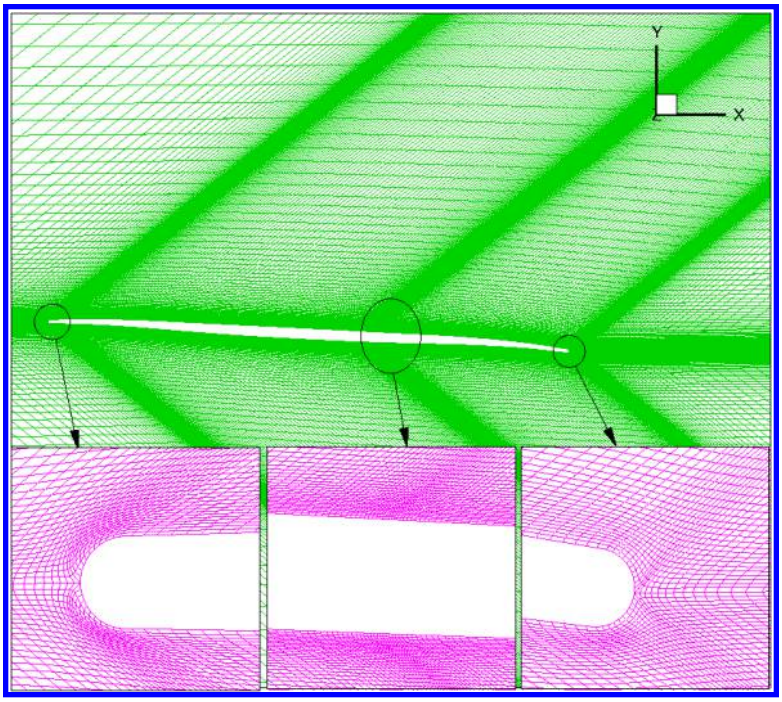

Figure 29: Zoomed refined mesh on the zero span plane to resolve the shock waves.

Fig. 34 is the wall surface isentropic Mach number distribution. It indicates that at zero span, the incidence is very small and the flow is mostly aligned with the leading edge metal angle. The

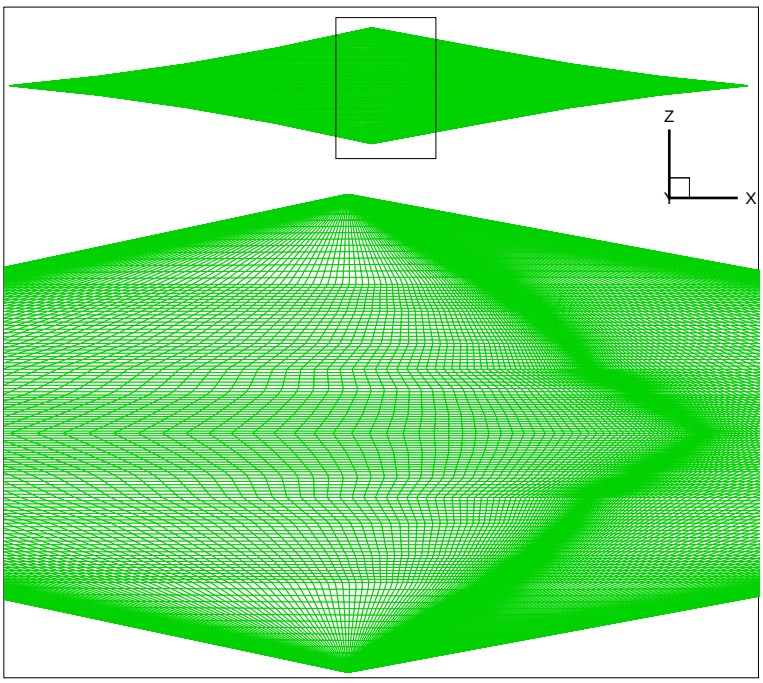

Figure 30: The refined mesh on suction surface with local refinement to resolve the shock along the span.

Table 10: D84-78.39, 0.1%

Length(m)	Span(m)	Area(m^2)	Volume(m^3)	AR(subsonic)	AR(supersonic)
100	15.7	688	544	14.580	0.357
Cl	Cd	Cl/Cd			
0.05551	0.00669	8.29746			
Altitude(ft)	36000	40000	50000	56000	60000
Noise(sBOOM, PLdB)	80.73	75.18	72.07	68.39	65.58

surface load distribution is fairly smooth with a sharp interruption at about 60% chord by the shock wave, which is not very strong due to the mitigated peak Mach number. The AoA is incresed toward the outer span and it generates very high peak Mach number. A strong shock wave emanates from the tip and intersects with the shock from the othet wing tip at the zero span. Improving the outspan flow to mitigate the peak Mach number may further reduce the ground sonic boom.

Fig. 35 is Mach number contours at different span showing the wave propagation in the near field. An oblique shock forms on the suction surface propagating upward and expansion wave on the pressure surface propagating downward followed by a shock wave. Fig. 36 is wall surface isentropic Mach number contours on the suction surface and pressure surface. The shock on the suction surface initiated from the wing tip is very well resolved, so is the expansion wave on the pressure surface.

The cross section airfoil shape at different streamwise locations is shown in Fig. 37, which is connected linearly by the airfoil st different span shown in Fig. 28. It is obviously not smooth. Since this work is focused on demonstrating the supersonic aerodynamic performance and sonic boom, no effort is made to smoothen the airfoil shape that will be used for subsonic flight. The

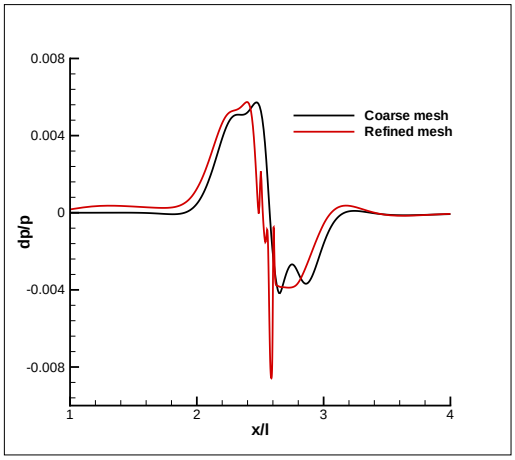

Figure 31: Pressure distribution 2 body length below at the zero span.

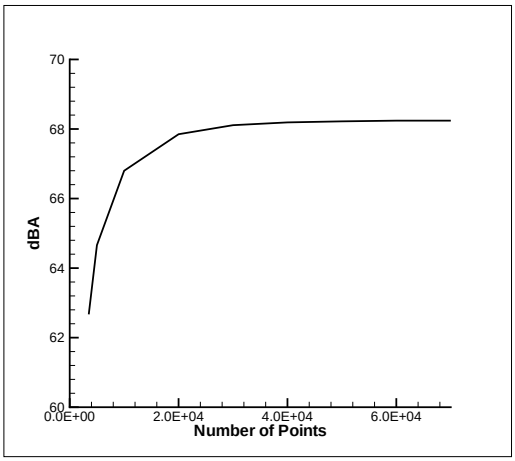

Figure 32: Grid convergence test for sBOOM wave propagation code.

future work will be considering the whole system.

Please note that all the designs in this study are created manually. It is believed that a systematic design optimization can significantly improve the design. Even though the design in this paper does not have the engine, it is believed that the primary sonic boom contribution is due to the lift, not the engine nacelles.

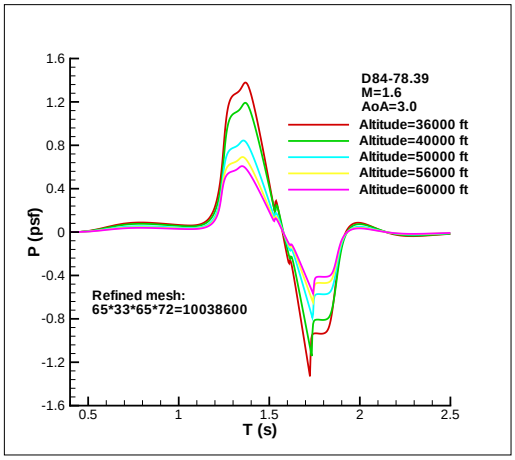

Figure 33: Ground sonic boom over-pressure signature for different flight altitude.

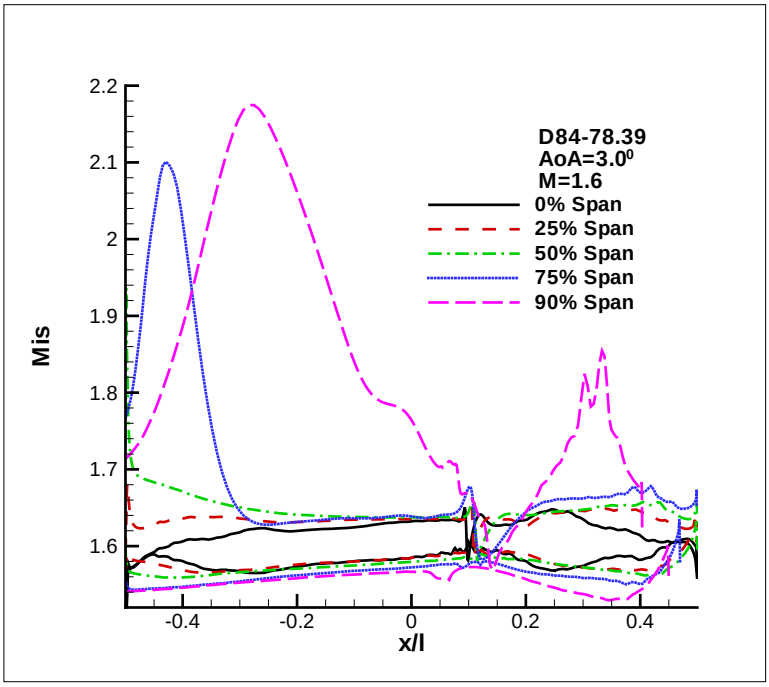

Figure 34: Isentropic mach number at different span

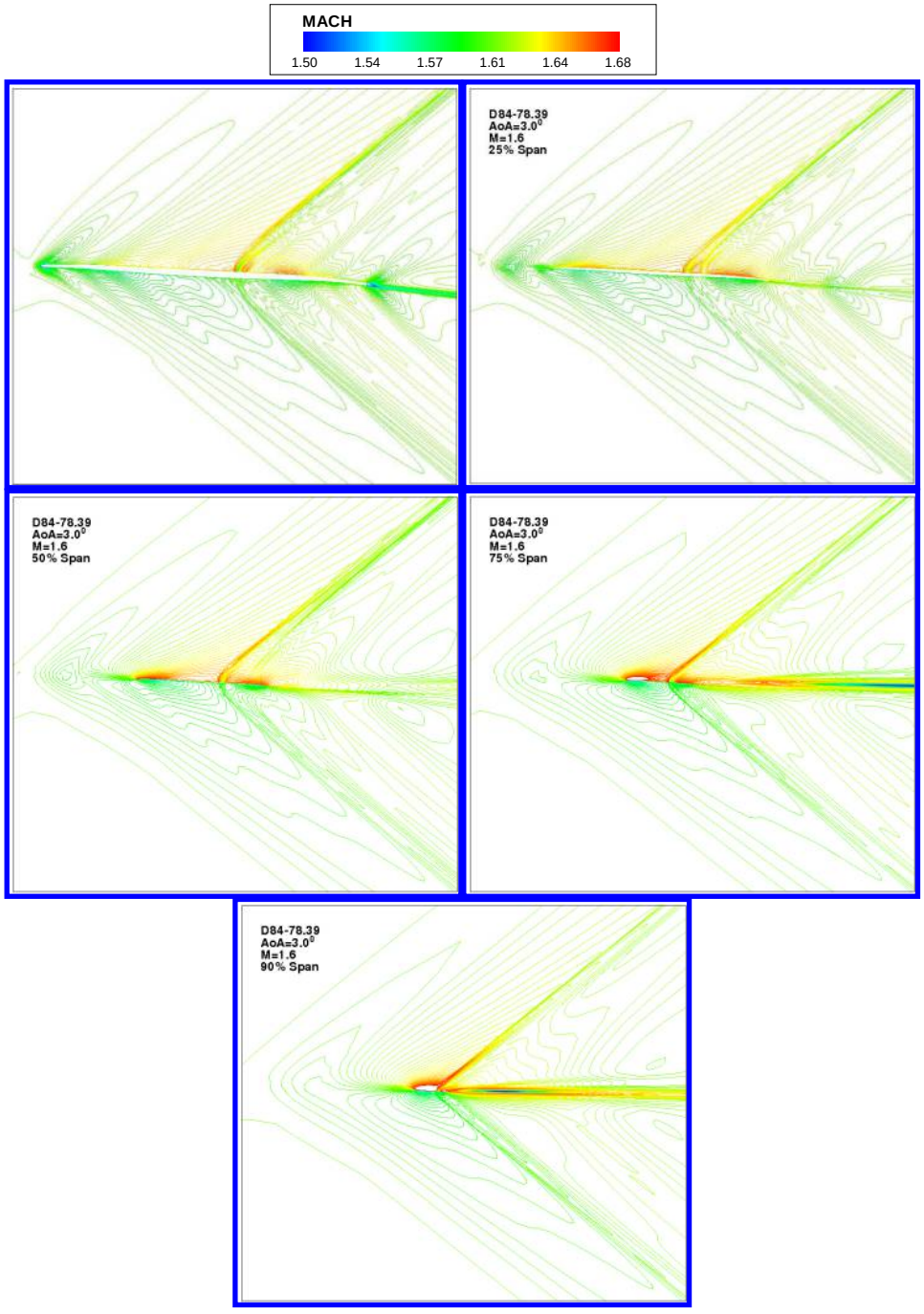

Figure 35: Isentropic Mach number contours at different spans

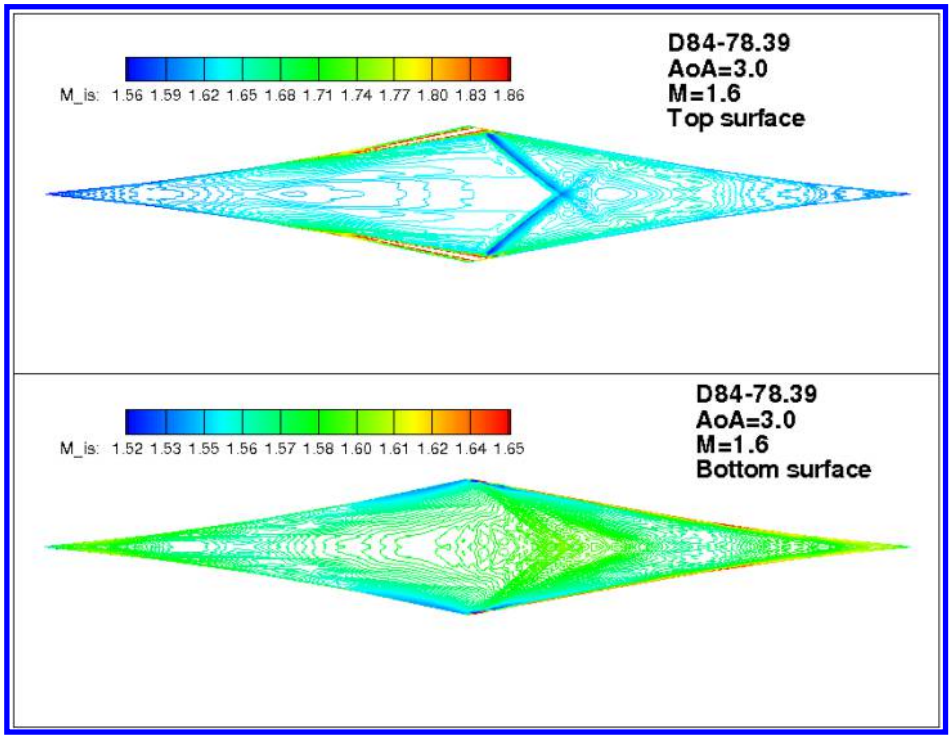

Figure 36: Surface isentropic Mach number with 0.1% zero-span-chord at tip

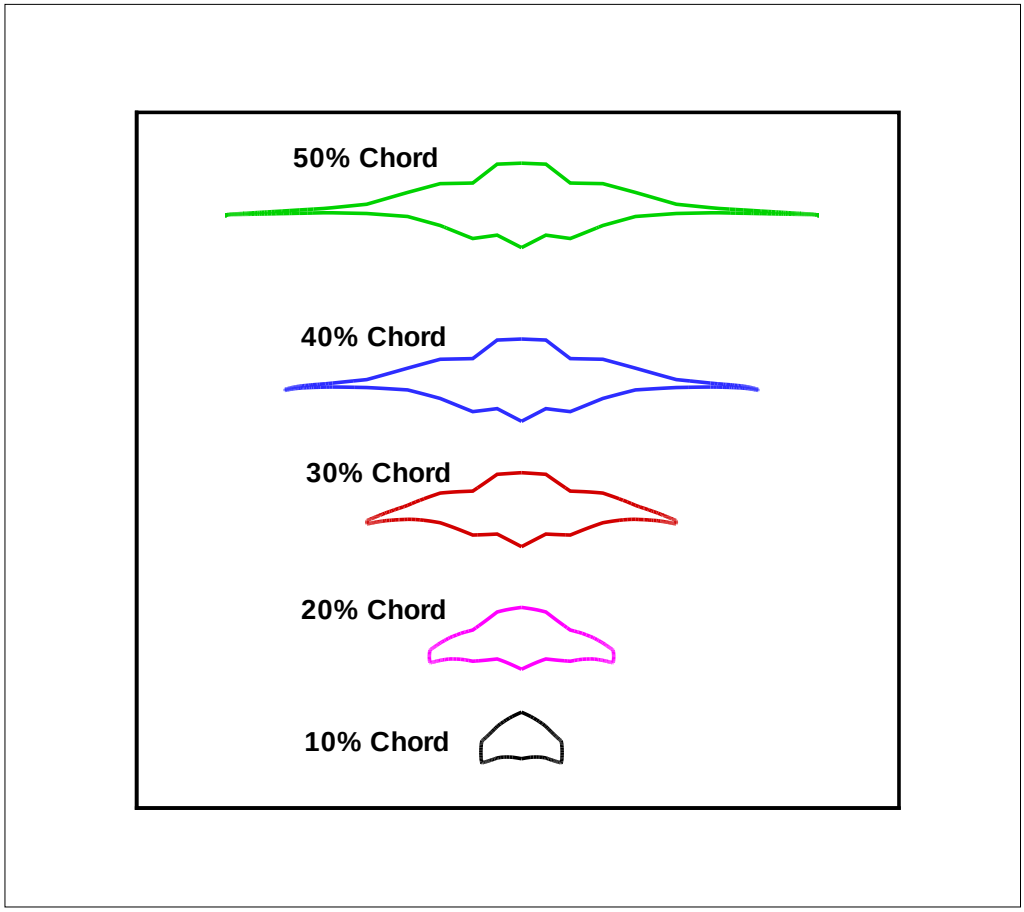

Figure 37: Airfoil shape of D84-78.39

7 Conclusions

This paper conducts a parametric trade study to establish and understand the relationship between the sonic boom/aerodynamic efficiency and the design parameters for supersonic bi-directional flying wing(SBiDir-FW). The mission requirements for this supersonic plane include the cruise Mach number of 1.6, range of 4000nm, payload of 100 passenger and flight altitude of 50k ft.

The concept can achieve high aerodynamic efficiency fairly straightforwardly. A design with variable sweep from 84° at the very leading edge to 68° at the tip achieves an a very high L/D of 10.4, which can be further increased if no sonic boom constraint is considered. The lift coefficient and L/D are primarily determined by the sweep angle distribution, which decides the SBiDir-FW planform and aspect ratio.

Reducing the sonic boom appears to be much more challenging. The trade study observes that the far field ground sonic boom signature is directly controlled by the smoothness of the loading and wave distributions on the airplane surface. The meanline angle distribution is a very effective control methodology to mitigate surface shock and expansion wave strength, and mitigating compression wave coalescing by achieving smooth loading distribution chord-wise. Compared with a linear meanline angle distribution, a design using non-monotonic meanline angle distribution in the mid-chord region with reversed cambering is able to reduce the sonic boom ground loudness by over 20PLdB. The sonic boom is sensitive to the angle of attack. When the AoA is deviated from the design AoA of 3° that gives the best L/D, the sonic boom is increased no matter the AoA is lower or higher. This is primarily because the variation of the AoA changes the front shock wave, which is minimized at the design AoA. Compared with the completely sharp LE and TE, the round LE and TE thickness has no harm to the sonic boom and aerodynamic performance. The d_{LE}/t_{max} up to 0.36, or $d_{LE}/chord$ of 0.8% is used in this design. The advantages using the round TE and LE are: 1) It significantly increases the airplane volume, up to 18% in this study. 2) It increases the tolerance of the airplane on AoA variation at both supersonic and subsonic mode.

The final design with refined mesh achieves sonic boom ground loudness of 72PLdB and aerodynamic dynamic efficiency L/D of 8.3. If increasing the cruise altitude from 50kft to 56kft and 60kft, the ground sonic boom loudness will be decreased to 68PLdB and 65PLdB respectively. The qualitative and quantitative findings in this paper give the understanding of physics and provide the path to achieve the ultimate high performance design. The SBiDir-FW concept indeed appears to be very promising to achieve high aerodynamic efficiency and low sonic boom. All the designs in this study are created manually. It is believed that a systematic automated design optimization will significantly improve the design performance further.

8 Acknowledgment

We are very grateful to NASA NIAC grant NNX12AR05G8 to study this new concept. We are particularly thankful to the program executive John (Jay) Falker and program manager Jason Derleth for their excellent leadership and strong support. We greatly appreciate the direction, discussion and team collaboration from L.Cattafesta and F. S. Alvi at Florida State University. We would like to thank S. Rallabhandi and M. Park for providing the sBOOM code. All the CFD simulation and design work are done at the Center for Computational Sciences(CCS) at

University of Miami.

References

[1] R. Seebass, " Sonic-Boom Theory ," *AIAA Journal of Aircraft*, vol. May-June, pp. 177–184, 1969.

[2] A. George and R. Seebass, " Sonic Boom Minimization including Both Front and Rear Shocks ," *AIAA Journal*, vol. 9, 10, pp. 2091–2093, 1971.

[3] R. Seebass and A. George, " Sonic-Boom Minimization ," *Journal of the Royal Aeronautical Society of America*, vol. 51, 2, pp. 686–694, 1972.

[4] Darden, C. M., "Minimization of Sonic-Boom Parameters in Real and Isothermal Atmospheres." NASA TN D-7842, March 1975.

[5] L. B. Jones, " Lower Bounds for Sonic Bangs ," *Journal of the Royal Aeronautical Society*, vol. 65, 606, pp. 433–436, 1961.

[6] Mack, R. J., and Needleman, K.E., "A Methodology for Designing Aircraft to Low Sonic Boom Constraints." NASA TM-4246, February 1991, 1991.

[7] Graham, D., "Quiet Supersonic Platform, Shaped Sonic Boom Demonstrator (SSBD) Program." FAA Civil Supersonic Aircraft Workshop, http://www.aee.faa.gov/Noise/aee100_files/SonicWkshp/2-Panel1-Graham-Northrop.pdf, Nov. 2003.

[8] Darden, C. M., "Sonic-Boom Minimization With Nose-Bluntness Relaxation." NASA TP-1348, January 1979.

[9] McLean, F. E., "Some Nonasymptotic Effects on the Sonic Boom of Large Airplanes." NASA TN D-2877, 1965.

[10] NASA, "NASA Research Announcement ROA-2008 Appendix A.4 Supersonics, Amendment 7, 1. Project Overview." 2008.

[11] Welge, H. R. and Nelson, C. and Bonet, J., "Supersonic Vehicle Systems for the 2020 to 2035 Timeframe." AIAA 2010-4930, 28th AIAA Applied Aerodynamics Conference, Chicago, Illinois, 28 June - 1 July 2010.

[12] Magee, T. E. and Shaw, S. G. and Fugal, S. R., "Experimental Validations of a Low-Boom Aircraft Design." AIAA 2013-0646, 51st AIAA Aerospace Sciences Meeting including the New Horizons Forum and Aerospace Exposition, Grapevine, TX, 07-10 Jan. 2013.

[13] Morgenstern, J. M.and Buonanno, M. and Nordstrud, N., "N+2 Low Boom Wind Tunnel Model Design and Validation." AIAA 2012-3217, 30th AIAA Applied Aerodynamics Conference, New Orleans, Louisiana, 25 - 28 June 2012.

[14] A. Jameson, "Optimum Aerodynamic Design Using CFD and Control Theory." AIAA 95-1729-CP, 1995.

[15] A. Jameson, "Aerodynamic Design via Control Theory," *Journal of Scientific Computing*, vol. 3, pp. 233–260, 1988.

[16] Alonso, J. J. and Kroo, I. M. and Jameson, A., "Advanced Algorithms for Design and Optimization of Quiet Supersonic Platforms." AIAA Paper 2002-0144, 2002.

[17] Choi, S. and Alonso, J. J. and Kroo, I. M. and Wintzer, M. , " Multi-Fidelity Design Optimization of Low Boom Supersonic Business Jets." AIAA 2004-4371, Aug. 30-Sept. 1, 2004.

[18] Rallabhandi, S. and Nielsen, E. J. and Diskin, B, "Sonic Boom Mitigation Through Aircraft Design and Adjoint Methodology." AIAA 2012-3220, 30th AIAA Applied Aerodynamics Conference, New Orleans, Louisiana, June 2012.

[19] Zha, G.-C. and Cattafesta, L. and Alvi, F. S. , "Silent and Efficient Supersonic Bi-Directional Flying Wing." Final Report for NASA NIAC Phase I Grant NNX12AR05G8, 9 July, 2013.

[20] Zha, G.-C., " Supersonic Flying Wing with Low Sonic Boom, Low Wave Drag, and High Subsonic Performance (SFW-L^{2}HSP)." Technology Transfer Office UMI-163, University of Miami,FL, Dec. 2008.

[21] Zha, G.-C., " Supersonic Bi-Directional Flying Wing." Provisional patent application No. 61172929, Submitted to USPTO, 27 Apr. 2009.

[22] Zha, G.-C., " Toward Zero Sonic-Boom and High Efficiency Supersonic UAS: A Novel Concept of Supersonic Bi-Directional Flying Wing." US Air Force Academic Outreach UAS Symposium, Grand Forks, ND, Aug. 4-6, 2009.

[23] Z.-J. Hu, M. Zha, G.-C.and Montgomery, T. Roecken, and J. Orosa, "Transonic Compressor Rotor Design Using Non-monotonic Meanline Angle Distribution." ASME Paper GT2007-27994, 2007.

[24] Zha, G.-C., Im, H. and Espinal, D., " Supersonic Bi-Directional Flying Wing, Part I: A novel concept for supersonic flight with high efficiency and low sonic boom ." AIAA Paper 2010-1013, 48th AIAA Aerospace Sciences Meeting, Orlando, FL, Jan. 4-6, 2010.

[25] Berger, C. and Carmona, K. and Im, H.-S. and Espinal, D.and Zha, G.-C., " Supersonic Bi-Directional Flying Wing Configuration with Low Sonic Boom and High Aerodynamic Efficiency." AIAA Paper 2011-3663, 29th AIAA Applied Aerodynamics Conference, Honolulu, Hawaii, 27-30 June 2011.

[26] Shen, Y.-Q. and Zha, G.-C. and Wang, B.-Y., " Improvement of Stability and Accuracy of Implicit WENO Scheme," *AIAA Journal*, vol. 47, No. 2, pp. 331–344, 2009.

[27] Shen, Y.-Q. and Zha, G.-C. , " Improvement of the WENO Scheme Smoothness Estimator," *International Journal for Numerical Methods in Fluids*, vol. DOI:10.1002/fld.2186, 2009.

[28] Shen, Y.-Q. and Zha, G.-C., " A Seventh-Order WENO Scheme and Its Applications." Submitted to SIAM Journal on Scientific Computing, Oct. 2010.

[29] B. Van Leer, "Towards the Ultimate Conservative Difference Scheme, III," *Journal of Computational Physics*, vol. 23, pp. 263–75, 1977.

[30] Y.-Q. Shen and G.-Z. Zha , "Generalized finite compact difference scheme for shock/complex flowfield interaction," *Journal of Computational Physics*, vol. doi:10.1016/j.jcp.2011.01.039, 2011.

[31] Shen, Y.-Q. and Zha, G.-C. and Chen, X.-Y., " High Order Conservative Differencing for Viscous Terms and the Application to Vortex-Induced Vibration Flows," *Journal of Computational Physics*, vol. 228(2), pp. 8283–8300, 2009.

[32] Y.-Q. Shen and G.-C. Zha, "Large Eddy Simulation Using a New Set of Sixth Order Schemes for Compressible Viscous Terms ," *Journal of Computational Physics*, vol. 229, pp. 8296–8312, 2010.

[33] P. Roe, "Approximate Riemann Solvers, Parameter Vectors, and Difference Schemes," *Journal of Computational Physics*, vol. 43, pp. 357–372, 1981.

[34] G.-C. Zha, Y. Shen, and B. Wang, "An improved low diffusion E-CUSP upwind scheme ," *Journal of Computer & Fluids*, vol. 48, pp. 214–220, 2011.

[35] Im, H-S., Chen, X-Y and Zha, G-C., " Detached Eddy Simulation of Rotating Stall Inception for a Full Annulus Transonic Rotor ," *AIAA Journal of Propulsion and Power*, vol. 28, No. 4, pp. 782–798, 2012.

[36] Im, H-S., Chen, X-Y., and Zha, G-C., "Prediction of a Supersonic Wing Flutter Boundary Using a High Fidelity Detached Eddy Simulation." AIAA Paper 2012-0039, 50th AIAA Aerospace Sciences Meeting, Tennessee,TN, submitted to AIAA Journal, 9-12 January 2012.

[37] Wang, B. Y and Zha, G.-C., "Detached-Eddy Simulation of Transonic Limit Cycle Oscillations Using High Order Schemes," *Journal of Computer & Fluids*, vol. 52, pp. 58–68, 2011.

[38] Wang, B. Y and Zha, G.-C., "Detached-Eddy Simulation of a Co-Flow Jet Airfoil at High Angle of Attack," *AIAA Journal of Aircraft*, vol. 48, 5, pp. 1495–1502, 2011.

[39] Im, H. and Zha, G., "Delayed Detached Eddy Simulation of the Aerodynamic Stall Flows Over the NACA0012 Airfoil." AIAA Paper 2011-1297, 49th AIAA Aerospace Sciences Meeting including, Orlando, Florida, 4 - 7 Jan 2011.

[40] Im, H-S. Chen, X.-Y. and Zha, G-C., "Simulation of 3D Multistage Axial Compressor Using a Fully Conservative Sliding Boundary Condition." ASME-IMECE 2011-62049, Proceedings of the ASME 2011 International Mechanical Engineering Congress & Exposition IMECE2011, Denver, Colorado, USA, Nov. 11-17, 2011.

[41] Im, H-S., Chen, X-Y and Zha, G-C., " Detached Eddy Simulation of Transonic Rotor Flutter Using a Fully Coupled Fluid-Structural Interaction ." ASME Paper GT2011-45437, ASME TURBO EXPO 2011, June 6-10, Vancouver, Canada, June 6-10, 2011.

[42] Im, H-S. and Zha, G-C., "Investigation of Co-Flow Jet Airfoil Mixing Mechanism Using Large Eddy Simulation." AIAA Paper 2011-3098, submitted to ASME J. of Fluid Engineering, (41st AIAA Fluid Dynamics Conference and Exhibit, 27-30 June 2011, Honolulu, Hawaii),, 2011.

[43] Wang, B. Y and Zha, G.-C., "High Fidelity Simulation of Nonlinear Fluid-Structural Interaction with Transonic Airfoil Limit Cycle Oscillations," *Journal of Fluids and Structures*, vol. doi:10.1016/j.jfluidstructs.2010.02.003, 2010.

[44] Wang, B.-Y. and Haddoukessouni, B. and Levy, J. and Zha, G.-C., "Numerical Investigations of Injection Slot Size Effect on the Performance of Co-Flow Jet Airfoil ," *AIAA Journal of Aircraft*, vol. 45, pp. 2084–2091, 2008.

[45] X.-Y. Chen, G.-C. Zha, and M.-T. Yang, "Numerical Simulation of 3-D Wing Flutter with Fully Coupled Fluid-Structural Interaction," *Journal of Computers & Fluids*, vol. 36, No. 5, pp. 856–867, 2007.

[46] X.-Y. Chen and G.-C. Zha, "Fully Coupled Fluid-Structural Interactions Using an Efficient High Resolution Upwind Scheme," *Journal of Fluids and Structures*, vol. 20, pp. 1105–1125, 2005.

[47] Z.-J. Hu and G.-C. Zha, "Calculations of 3D Compressible Using an Efficient Low Diffusion Upwind Scheme," *International Journal for Numerical Methods in Fluids*, vol. 47, pp. 253–269, 2004.

[48] Im, H-S. and Zha, G-C., "Effects of Rotor Tip Clearance on Tip Clearance Flow Potentially Leading to NSV in an Axial Compressor." ASME Paper GT2012-68148, IGTI Turbo Expo 2012, Copenhagen, Denmark, June 11-15, 2012.

[49] Im, H-S. and Zha, G-C., "Simulation of Non-synchronous Blade Vibration of an Axial Compressor Using a Fully Coupled Fluid-Structural Interaction." ASME Paper GT2012-68150, IGTI Turbo Expo 2012, Copenhagen, Denmark, June 11-15, 2012.

[50] Chen, X-Y., Im, H-S., and Zha, G-C., "Fully Coupled Fluid-Structural Interaction of a Transonic Rotor at Near-Stall Conditions Using Detached Eddy Simulation." AIAA Paper 2011-0228, 49th AIAA Aerospace Sciences Meeting including the New Horizons Forum and Aerospace Exposition 4 - 7 January 2011, Orlando, Florida, submitted to AIAA Journal, 2011.

[51] B.-Y. Wang and G.-C. Zha, "A General Sub-Domain Boundary Mapping Procedure For Structured Grid CFD Parallel Computation," *AIAA Journal of Aerospace Computing, Information, and Communication*, vol. 5, No.11, pp. 2084–2091, 2008.

[52] Winter, K. G. and Smith, K. G., "Measurements of Skin Friction on a Cambered Delta Wing at Supersonic Speeds." R. & M. No. 3501, AERONAUTICAL RESEARCH COUNC1L, LONDON, HER MAJESTY'S STATIONERY OFFICE, August 1965.

[53] Park, M. A., "Low Boom Configuration Analysis with FUN3D Adjoint Simulation Framework." AIAA 2011-3337, 29th AIAA Applied Aerodynamics Conference, Honolulu, Hawaii, June 2011.

[54] Seebass, R., "Supersonic Aerodynamics: Lift and Drag ." Paper presented at the RTO AVT Course on *Fluid Dynamics Research on Supersonic Aircraft*, RTO EN-4, Rhode-Saint-Gendse, Belgium,, 25-29 May 1998.

[55] Durston, D. A. , " Sonic Boom Extrapolation and Sound Level Prediction." Unpublished Document, NASA Ames Research Center, Sept. 2009.

[56] Corke, T. C., *Design of Aircraft*. Prentice Hall, 2003.

[57] Rallabhandi, S. K., "Advanced Sonic Boom Prediction Using Augmented Burgers Equation." 49th AIAA Aerospace Sciences Meeting including the New Horizons Forum and Aerospace Exposition, Orlando, Florida, Jan. 4-7, 2011.